Reactive oxygen species modulate macrophage immunosuppressive phenotype through the up-regulation of PD-L1

Reactive Oxygen Species modulate macrophage immunosuppressive phenotype through the up-regulation of PD-L1

Cecilia Roux[ab], Soode Jafari[a], Rahul Shinde[a], Gordon Duncan[a], David W. Cescon[a], Jennifer Silvester[a], Mandy Fang-chi[a], Kelsey Hodgson[a], Thorsten Berger[a], Andrew Wakeham[a], Luis Palomero[c], Mar Garcia-Valero[c], Miguel A. Pujana[c], Tak W. Mak[a], Tracy L. McGaha[a], Paola Cappello[d]* and Chiara Gorrini[a]*

[a]The Campbell Family Institute for Breast Cancer Research at Princess Margaret Cancer Centre, 610 University Avenue, Toronto, ON M5G 2M9, Canada
[b]Molecular Biotechnology Center, University of Turin, Via Nizza 52, 10126 Turin, Italy
[c]Breast Cancer and Systems Biology Laboratory, Program Against Cancer Therapeutic Resistance (ProCURE), Catalan Institute of Oncology (ICO), Bellvitge Institute for Biomedical Research (IDIBELL), L'Hospitalet del Llobregat, Barcelona 08908, Catalonia, Spain
[d]Department of Molecular Biotechnologies and Health Science, University of Turin, Via Nizza 52, 10126 Turin, Italy

*To whom correspondence should be addressed. Email: paola.cappello@unito.it, Chiara.Gorrini@uhnresearch.ca

Lead Contact Information:

Chiara Gorrini, PhD
The Campbell Family Institute for Breast Cancer Research
610 University Avenue, 8th floor, rm 509, Toronto, ON M5G 2M9, Canada
Phone: 416-946-4501#4022
Email: Chiara.Gorrini@uhnresearch.ca

ABSTRACT

The combination of immune checkpoint blockade with chemotherapy is currently under investigation as a promising strategy for the treatment of Triple Negative Breast Cancer (TNBC). Tumor-associated macrophages (TAM) are the most prominent component of breast cancer microenvironment because they influence tumor progression and the response to therapies. Here we show that macrophages acquire an immunosuppressive phenotype and increase the expression of programmed death ligand-1(PD-L1) when treated with reactive oxygen species (ROS) inducers such as the glutathione synthesis inhibitor BSO and paclitaxel. Mechanistically, these agents cause accumulation of ROS that in turn activate NF-kB signalling to promote PD-L1 transcription and the release of immunosuppressive chemokines. Systemic *in vivo* administration of paclitaxel promotes PD-L1 accumulation on the surface of tumor-associated macrophages in a mouse model of TNBC, consistent with *in vitro* results. Combinatorial treatment with Paclitaxel and an anti-mouse PD-L1 blocking antibody significantly improved the therapeutic efficacy of paclitaxel by reducing tumor burden and increasing the number of tumor-associated cytotoxic T cells. Our results provide a strong rationale for the use of anti-PD-L1 blockade in the treatment of TNBC patients. Furthermore, interrogation of chemotherapy-induced PD-L1 expression in TAM is warranted to define appropriate patient selection in the use of PD-L1 blockade.

SIGNIFICANCE STATEMENT

Immunotherapies targeting the programmed death-1 (PD-1) and its ligand PD-L1 have recently been combined with standard chemotherapy to potentiate the treatment of solid tumors, including Triple Negative Breast Cancer (TNBC). Reactive Oxygen Species (ROS) have been directly linked to the cytotoxic effects of chemotherapy. Here we report that ROS induced either by chemotherapy (paclitaxel) or antioxidant depletion induce PD-L1 expression in macrophages. PD-L1-positive macrophages have immune-suppressive and angiogenic properties that interfere with the efficacy of paclitaxel *in vivo*. Indeed, PD-L1 blockade reverts this effect and synergizes with paclitaxel to reduce tumor growth. Our work reveals a novel pathway that further supports the importance of combining taxane and PD-L1 inhibitors as promising anti-cancer strategy in TNBC.

\body

INTRODUCTION

Triple-Negative Breast Cancer (TNBC) is an aggressive heterogeneous disease, which includes up to 20% of breast cancers (BC). Clinical treatment of this disease is particularly challenging and is currently limited to standard chemotherapy(1). Although TNBC are particularly sensitive to neoadjuvant chemotherapy with pathological complete response (pCR) rates of about 40%, these cancers maintain a high rate of relapse(2).

TNBC was initially classified among the non-immunogenic “cold” tumors but recent studies have proved that the expression of immune-related genes and the presence of immune infiltrates in primary lesions are associated with a better clinical outcome(3, 4). TNBC is also characterized by genomic instability and high rates of genetic mutations, which implicate production of more neo-antigens and increased immunogenicity(5). These findings have encouraged the development of new combinatory strategies between chemotherapy and immune checkpoint inhibitors targeting the programmed death-1 (PD-1) and its ligand (PD-L1)(6). In these settings, the use of PD-1/PD-L1 inhibitors could elicit or potentiate the antitumor response induced by chemotherapy(6). Indeed, ongoing clinical trials have shown that immune checkpoint blockade in combination with neoadjuvant chemotherapy correlates with an increased pathological complete response rates in TNBC patients(7). Although these clinical studies are reporting encouraging data on the efficacy of chemo-immunotherapy, basic understanding of the interplay between chemotherapy and immunotherapy is limited.

Among the most urgent needs, it is the characterization of biomarkers for a better stratification of TNBC patients in the response to these combinatorial strategies(8, 9). In some studies, PD-L1 expression have been evaluated by IHC in both cancer and stromal cells with the indication that PD-L1 expression among tumor-infiltrating immune cells may be a better robust predictor(7). Indeed, a recent work has found that analysis of PD-L1 levels on both cell types is necessary for predicting best response to atezolizumab (PD-L1 inhibitor) in non-small cell lung cancer(10). Being a cell surface protein, it is conceivable that the expression of PD-L1 is regulated by external stresses in the tumor microenvironment (TME) and may represent a key node at the interface of extracellular and intracellular cancer signaling pathways.

A well characterized mediator of chemotherapy-induced cytotoxicity is the accumulation of reactive oxygen species (ROS) in cancer and stromal cells(11, 12). In TNBC, tumor-associated macrophages (TAM) support tumor progression and are potent regulator of therapeutic response in BC because they can suppress immune-based mechanism of

cytotoxic chemotherapy(13, 14). Based on these considerations, we speculated that chemotherapy-induced ROS could affect the expression of PD-L1 in macrophages and the immune properties of the TME.

Here we report that ROS induced by the glutathione synthesis inhibitor, BSO positively regulates mRNA and protein surface expression of PD-L1 in human and mouse macrophages *in vitro*. These macrophages also produce immunosuppressive cytokines including IL-4, IL-10 and IL-17 and the angiogenic factor, Vascular Endothelial Growth Factor-A (VEGF-A). Interestingly, the chemotherapeutic drug and ROS inducer, paclitaxel, reproduced all BSO-mediated effects in macrophages. Furthermore, in mouse BRCA1/p53-deleted mammary tumors, a model which resembles spontaneous TNBC, *in vivo* administration of paclitaxel induced PD-L1 expression in TAM as soon as 24h after treatment, leading to an immunosuppressive TME. Consequently, the *in vivo* combination of paclitaxel and an anti-PD-L1 blocking antibody reduced mammary tumor burden and reverted the immune-properties of TME. Our data show that ROS are novel regulators of PD-L1 expression, immune-suppressive and angiogenic features of macrophages. This study emphasises the importance of evaluating PD-L1 expression in TAM as predictive biomarker of chemo-immunotherapy response in TNBC patients.

RESULTS

ROS regulate PD-L1 expression and secretion of immunosuppressive cytokines in macrophages *in vitro*

Recent work has shown that in tumor-bearing mice, tumor-associated macrophages (TAM) expressed much higher surface levels of PD-L1 than circulating monocytes, implying upregulation of PD-L1 by the tumor microenvironment(15). ROS generation and accumulation in TME have important implications in the initiation and progression of cancer(12). To elucidate if ROS could regulate the expression of PD-L1 in macrophages, we treated bone marrow-derived macrophages (BMDM) with BSO, which increases ROS by depleting reduced glutathione (GSH)(16). BSO positively induced PD-L1 mRNA levels in a ROS-dependent manner since its effect was reverted by co-treatment with the antioxidant and ROS quencer N-acetyl-cysteine (NAC) (Fig. 1*A*). This change coincided with modulation of intracellular ROS levels as shown by quantification of DCF-DA staining by flow cytometry (*SI Appendix* Fig. 1*A*). BSO-mediated effect on PD-L1 expression was greater when BMDM were first treated with IL-4 and M-CSF that polarize them toward alternatively-activated

macrophages with features similar to TAM (17) (*SI Appendix* Fig. S1*B*). The polarization of these BMDM was confirmed by the elevated expression of Arginase-1(17) (*SI Appendix* Fig. S1*C*).

BSO also triggered the expression of the NRF2 antioxidant targets, *Gclc*, *Gclm, Nqo1* and *Hmox-1* as a response to the intracellular redox imbalance (Fig. 1*B* and *SI Appendix*, Fig. S1*D*). Data in mouse BMDM were validated in human monocyte-derived macrophages treated with BSO with or without NAC. Human macrophages increased PD-L1 mRNA levels as well as NRF2 target, *NQO1,* as a response to different ROS conditions (*SI Appendix*, Fig. S1*E, F).*

Next, we investigated which population among BMDM was mainly affected by BSO in terms of PD-L1 protein surface expression. In BSO-treated mouse BMDM defined as CD11b and F4/80 double-positive cells ($CD11b^{+}F4/80^{+}$), PD-L1 expression was not affected by the presence of BSO (*SI Appendix*, Fig. S1*G*), but it completely coincided with a population characterized by high positivity of mannose receptor C type 1 (MRC1/CD206) and absence of expression of major histocompatibility complex class II (MHC-II) molecules (Fig. 1*C* and *SI Appendix*, Fig. S1*H, I*) Of note, the $CD206^{+}MHC\text{-}II^{-}$ macrophages are usually defined as alternatively-activated macrophages. (14, 18). By contrast, PD-L1 expression was almost unchanged in a population highly expressing MHC II ($CD206^{-}MHC\ II^{+}$)(Fig. 1*D* and *SI Appendix*, Fig. S1*H,I*). In human macrophages, PD-L1 surface staining increased in $CD11b^{+}$ cells upon BSO and decreased when NAC was added to the culture (*SI Appendix*, Fig. S1*J*). PD-L1 expression has been previously associated with the immune-suppressive features of macrophages(19). Therefore, we analysed which cytokines were present in the media of BSO- and BSO±NAC-treated mouse BMDM by applying a mouse cytokine antibody array. We found that, compared to untreated cells, BSO stimulated production of Interleukin-10 (IL-10), Interleukin-17 (IL-17), Interleukin-4 (IL-4), Interleukin-1 beta (IL-1b), Insulin-like growth factor-binding protein 3 (IGFBP-3) and chemokine (C-X-C motif) ligand 1 (CXCL1) (Fig. 1*F*). IL-10, IL-4, IGFBP-3 and CXCL1 are usually associated to an immune-suppressive phenotype of macrophages(20-23). IL-1b is a well-known pro-inflammatory cytokine that has been associated with breast cancer progression and ability to metastasize, especially to extravasate when induced by neutrophils with metalloproteases and other pro-inflammatory cytokines(24, 25). IL-17 is another inflammatory cytokines but it can enhance immunosuppression in several systems including macrophages(26). On the other hand, BSO-treated BMDM produced low levels of Interleukin-12 isoform (IL-12) p40/p70 heterodimer and p40 monomer, as well as CD30L (TNFRSP8), CD40 and C-X-C motif

chemokine 10 (CXCL-10) (Fig. 1*E*). Overall, these data suggest that ROS drive a phenotypic change in macrophages characterized by reduced antigen presenting function and co-stimulatory ability (27-29). In the same cells, ROS also upregulated the production of VEGF-A, indicative of angiogenic macrophages(30). Notably, NAC completely reverted the production of cytokines and VEGF-A induced by BSO, indicating a key role of ROS in these changes (Fig. 1*E*).

ROS induction is a key component of the cytotoxic properties of chemotherapy(11). We compared three chemotherapeutic drugs for their ability to increase ROS in BMDM: the antimitotic agent paclitaxel, the poli ADP-ribosil polimerase (PARP) inhibitor olaparib and the platinum-based drug cisplatin (1). Compared to cisplatin and olaparib, paclitaxel induced the highest ROS levels in BMDM (*SI Appendix*, Fig. S2*A*). In contrast to cisplatin and olaparib, paclitaxel did not cause any DNA damage as measured by intracellular accumulation of phosphorylated H2AX (γH2AX) (*SI Appendix*, Fig. S2*B*)(31). Paclitaxel-induced ROS levels were not cytotoxic since BMDM had similar cellular viability in both untreated and treated conditions as measured by the sulforhodamine B (SRB) assay (*SI Appendix*, Fig. S2*C)*. Given its ability of elevating ROS, paclitaxel triggered the expression of *Pdl1* as compared to control cells that was reverted when ROS were scavenged by NAC (Fig. 1*F* and *SI Appendix*, Fig. S2*D*). Similarly to BSO, paclitaxel-mediated effect on PD-L1 expression was augmented by polarization of BMDM toward alternatively-activated macrophages (*SI Appendix*, Fig. S2*E*). NRF2-regulated antioxidant genes, *Gclc*, *Gclm* and *Hmox1* were also elevated in paclitaxel-treated BMDM (Fig. 1G and SI *Appendix*, Fig. S2*F*). Flow cytometry analysis also showed increased levels of PD-L1 specifically on the surface of $CD206^{+}$ $MHC\text{-}II^{-}$ upon treatment with paclitaxel that was reduced by adding NAC (Fig. 1*H* and *SI Appendix*, Fig. S2*G*). On the contrary, $CD206^{-}MHC\text{-}II^{+}$ BMDM did not show any change (Fig. 1I and *SI Appendix*, Fig. S2*G*). Analysis of human macrophages recapitulated the elevation of both PD-L1 mRNA and surface protein after exposure to paclitaxel that was reverted by NAC (*SI Appendix*, Fig. S2*H*,*I*). The expression of the NRF2 antioxidant enzyme *NQO1* was similarly regulated (*SI Appendix*, Fig. S2*J*). Then, we analysed the cytokine and growth factor production of BMDM treated with paclitaxel with or without NAC. Interestingly, media from paclitaxel-stimulated BMDM contained the same profile of cytokines observed after BSO treatment (Fig. 1*J*). In addition, we detected Fas ligand (Fasl) and C-X3-C Motif Chemokine Ligand (CX3CL1) (Fig. 1*J*). Fasl is a common mediator of apoptosis in T cells expressing the receptor Fas, whereas CX3CL1 functions as an adhesion molecule(32, 33).

The production of these cytokines was significantly reverted by co-treatment with NAC (Fig. 1*J*).

ROS-induced PD-L1 expression is mediated by the transcription factor NF-kB

We noted that most of the cytokines induced by BSO and paclitaxel treatments have been previously characterized as transcriptional targets of the transcription factor NF-kB (https://www.bu.edu/nf-kb/gene-resources/target-genes/). Furthermore, it is known that activation of NF-kB can promote cell survival and prevent oxidative damage in response to ROS(34). Thus, we hypothesized that ROS might regulate PD-L1 expression through NF-kB activation.

NF-kB molecular forms are usually dimers and the dimer formation is necessary for DNA binding. The most abundant form of NF-kB dimer is p50/p65 heterodimer that mediates the canonical activation of the pathway(35). Upon phosphorylation on the two key residues, S276 and S536, p65 undergoes to a conformational change that triggers its transcriptional activity(35). In BSO- and paclitaxel-treated BMDM we found an increased frequency of cells positive for the phosphorylation of p65 at S536 residue by immunofluorescence staining (Fig. 2*A* and *SI Appendix*, Fig. S3*A*). The number of these cells was reduced by co-treatment with either the ROS quencher NAC or the nuclear factor kappa-B kinase-2 (IKK-2) inhibitor SC514 (Fig. 2*A* and *SI Appendix*, Fig. S3*A*)(36). Treatment with lipopolysaccharides (LPS) was used as positive control of p65 phosphorylation in BMDM (Fig. 2*A*)(37). These results were validated by measurement of P-p65 overall nuclear intensity in the same conditions (Fig. 2*B* and *SI Appendix*, Fig. S3*B*). We further verified the activation of NF-kB pathway by analysing the expression of the NF-kB target gene, *IkBa*. *IkBa* mRNA was up-regulated by BSO and paclitaxel treatments and the effect was reverted by NAC and SC514 co-treatments (Fig. 2*C*). Strikingly, SC514 also reduced *Pdl1* mRNA in BSO- or paclitaxel-treated BMDM (Fig. 2*D*). Then we sought to validate that SC514-mediated effect on PD-L1 was indeed mainly NF-kB dependent. To do so, we analysed the expression of *IkBa*, vascular endothelial factor-A (*Vegfa*) and *PD-L1* in BMDM treated with BSO and paclitaxel combined with an inhibitor of aryl-hydrocarbon receptor (AhRi). AhR is a transcription factor involved into ROS detoxification, growth factor signalling and can cross-talk with NF-kB pathway(38). AhR inhibition impaired BSO- and paclitaxel-regulated *Vegfa* as previously described(39, 40)but did not affect *IkBa* or *Pdl1* increased levels (*SI Appendix*, Fig. S3*C*).

SC514 also affected PD-L1 cell surface expression in $CD206^{+}MHC\text{-}II^{-}$ BMDM (Fig. 2*E* and *SI Appendix*, Fig. S3*D*).

Our data showed a novel mode of regulation of PD-L1 by NF-kB via ROS. We found that ROS induced p65 phosphorylation at a level similar to LPS (Fig. 2*A*,*B*). PD-L1 has been previously identified to be regulated in BMDM by LPS-induced NF-kB activation (41). By analyzing the same gene dataset, we confirmed that PD-L1 expression increased in LPS-treated BMDM and positively correlated with *Nfkb1/p65* and Rela/p50 mRNA levels (*SI Appendix*, Fig. S3*E*). Moreover, the link between NF-kB and mouse PD-L1 gene transcription was reinforced by the identification of a Nfkb1/p65 binding enhancer (I1551) through bioinformatics analysis of the inflammatory gene expression program in macrophages(42)(Fig. 1*F*). By chromatin immunoprecipitation followed by quantitative PCR (ChIP-qPCR) we found a significant enrichment of p65 at I1551 site in the *Pdl1* promoter at 1h after paclitaxel treatment that was reverted by NAC (Fig. 2*G*). In the same conditions, p65 failed to bind the promoter of the NF-kB target, IL-6, suggesting a specificity in gene transcription activation by NF-kB upon high ROS.

Paclitaxel promotes PD-L1 expression in tumor-associated macrophages *in vivo*

Through bioinformatics analysis of TCGA human database of both Basal BC and BC with homologous recombination DNA repair defects (HR-defective BC, see Materials and Methods for additional details), we found that cancer-associated PD-L1 positively correlated with an elevated infiltration of monocytic lineage cells (monocytes and macrophages) in the TME (*SI Appendix*, Fig. S4*A*)(43). To test if paclitaxel could induce PD-L1 expression in TAM, we took advantage of a mouse mammary tumor cell line carrying BRCA1/Trp53 deletion and resembling human TNBC (hereafter referred to as KBP)(44). These cells form palpable tumors once transplanted in the mammary fat pad of immune-proficient female mice, allowing analysis of both tumor and immune cell populations in the TME, including TAM. We administrated vehicle and paclitaxel intravenously at 20mg/kg to mice bearing tumors at a palpable and measurable size (70mm_3). Tumors were harvested and dissociated for flow cytometry analysis both at 24h and 5 days post-treatment. In $CD206^+MHC\ II_{low}$ TAM, PD-L1 surface expression did not change at 24h post-treatment but showed a significant increase at 5 days after paclitaxel injection, even if we noticed a slight increase of *Pdl1* in tumors from vehicle treated mice, likely due to the tumour mass progression from 70mm_3 to about 200-300mm_3 (Fig. 3*A* and *SI Appendix*, Fig. S4*B*). Indeed, *in vitro* co-cultured BMDM with KBP cells displayed an ncrease in *Pdl1* and arginase 1 (*Arg1*) expression after being in contact with tumor cells (*SI Appendix*, Fig. S4*C,D*. These results postulate that TAM are instructed *in situ* by tumour cells to express *Pdl1* during tumour progression. We found that

circulating monocytes in tumor bearing mice either untreated or paclitaxel-treated expressed very low to undetectable levels of PD-L1 (Fig. 3*B* and *SI Appendix*, Fig. S4*E*).

Then, we asked the question if PD-L1 expression correlated with ROS levels in CD206^{+}TAM as found in BMDM. At 5 days post-treatment, we stained CD206^{+}TAM for DCF-DA to measure intracellular ROS. Strikingly, we observed an increased positivity for DCF-DA in the PD-L1^{+} macrophages, validating the link between cellular redox status and PD-L1 levels found *in vitro* (Fig. 3*C*). It is reported that paclitaxel treatment is also able to induce PD-L1 expression in tumor cells, including the TNBC cell line MDA-MB-231 and a panel of ovarian cell lines(45-47). Therefore, we investigated PD-L1 levels in CD45^{-}CD49f^{+} KBP mammary tumor cells as we did in TAM. We did not observe any increased PD-L1 positivity within mammary tumor epithelial cells, either 24h or 5 days post treatment (Fig. 3*D* and *SI Appendix*, Fig. S4*F*). *In vitro* treatment of same KBP cells with increasing doses of paclitaxel induced a very marginal increase in PD-L1 surface expression after 24h (*SI Appendix*, Fig. S4*G*). Consistent with the *in vitro* results from BMDM cytokine array, TAM from paclitaxel-treated tumors produced higher levels of IL-10 and IL-17 and lower amount of IL-12 (Fig. 4*E*-G and *SI Appendix* S4*H*).

To investigate the involvement of NF-kB in PD-L1^{+} TAM *in vivo*, we analysed CD206^{+} PD-L1^{+} TAM for the presence of phosphorylated p65 in both paclitaxel-and vehicle-treated KBP allografts. At 5 day time point, when PD-L1 surface expression was high, these macrophages also showed an increase in p65 phosphorylation, suggesting activation of NF-kB pathway in the same cellular compartment (Fig. 3*E* and *SI Appendix*, Fig. S4*H*). Overall, both *in vitro* and *in vivo* data elucidate a link between paclitaxel, ROS accumulation and NF-kB activation in macrophages. We corroborated this signaling pathway by bioinformatics analysis of TCGA Basal and HR-defective BC cohorts. In these datasets, we looked for correlation between expression signature of human BC-infiltrating TAM(48, 49), our key genes of interest (i.e., *PD-L1* and *NFKB1/p65*) and a comprehensive ROS-induced gene signature(50). We investigated gene correlations in the expression profiling of both M1 and M2 compartments identified in the two published studies(48, 49). These studies elucidated that macrophages express M1 and M2-type gene modules simultaneously and M1 and M2 genes positively correlate in macrophages, contrary to models supporting mutually exclusive M1 and M2 subsets(49). We found that in both Basal and HR-defective BC cohorts, M1 and M2 signatures positively correlated with expression of PD-L1, NFKB1/p65 and activation of ROS signaling pathway (Fig. 3*F* and *SI Appendix*, Fig. S4*I*).

PD-L1 blockade potentiates anti-tumor effects of paclitaxel *in vivo*

Several ongoing clinical trials in TNBC patients are currently exploring the effectiveness of combining paclitaxel treatment with immune checkpoint inhibitors as compared to single agent therapy(7, 51, 52). We hypothesized, based on our *in vitro* and *in vivo* observations, that inhibition of PD-L1 could revert the immune-suppressive and tumorigenic properties of TAM to enhance the anti-tumor activity of paclitaxel. We first assessed if the use of anti-PD-L1 antibody (αPD-L1) could affect the viability of BMDM whether alone or in combination with paclitaxel *in vitro* by SRB assay. Isotype-treated cells were included as control. We did not notice any difference in cell viability in both groups over 5 days treatment (*SI Appendix*, Fig. S5*A*). In addition, we did not find any changes in the surface expression of CD206 and MHC-II, in both treated- or control cells (*SI Appendix*, Fig. S5*B,C*). αPD-L1 also did not affect paclitaxel-induced *Pdl1* mRNA increase (*SI Appendix*, Fig. S5*D*).

Then, we investigated if PD-L1 blockade could influence the production of cyokines in BMDM. Interestingly, we found that PD-L1 inhibition restored all the paclitaxel-induced cytokines to control level (Fig. 4*A*). *Vegfa* mRNA levels were also negatively affected by αPD-L1/paclitaxel combination compared to isotype/paclitaxel (Fig. 4*B*).

These *in vitro* data prompted us to investigate the anti-tumor effect of αPD-L1 in the KBP mouse model in combination with paclitaxel. We administrated paclitaxel (intravenously) and αPD-L1 (intraperitoneally) either in combination or as single agents. First, mice were treated with paclitaxel (to induce PD-L1) and then with αPD-L1 as summarized in Fig. 4*C*. Since paclitaxel was administrated once a week, we performed an additional injection of αPD-L1 to guarantee PD-L1 blockade. Both compounds were administrated when mammary tumors reached a palpable and measurable volume (70mm_3). Tumor-bearing mice were monitored until they reached humane endpoint (tumor volume≤ 2cm_3). Combinatorial treatment of KBP mice with paclitaxel and αPD-L1 significantly reduced both tumor volume and weight as compared to control mice (Fig. 4*D,E*). On the contrary, the administration of either paclitaxel or αPD-L1 as monotherapy did not show any effect (Fig. 4*D,E*). Haemotoxylin and Eosin (H&E) staining of KBP allografts showed that all treated tumors had a reduced mitotic index compared to tumors from vehicle+isotype mouse group (Fig. 4*H*). We did not find any difference in blood vessel density based on immunohistochemical staining of the platelet endothelial cell adhesion molecule PECAM1/CD31 (*SI Appendix*, Fig. S5*E*). Compared to paclitaxel alone, co-treatment with PD-L1 blockade significantly impaired P-p65 signal and increased cleaved caspase 3 (Fig. 4*I*,*J* and *SI Appendix*, Fig. S5*F,G*).

Paclitaxel combined with PD-L1 blockade leads to anti-tumor immune activation

To evaluate the immune response in the KBP allografts, we collected and analysed tumors from all mouse group at endpoint for immune cell infiltrates. We observed a moderate reduction in the percentage of F4/80+/CD11b+TAM in the αPD-L1/paclitaxel group, probably due to reduced infiltration in the TME rather than increased TAM cell death (Fig. 5*A*). Then, we looked at the impact of αPD-L1/paclitaxel regimen on different T cell populations. aPD-L1/paclitaxel-treated tumors restored the number of CD4+T cell that were reduced by paclitaxel alone (*SI Appendix* Fig. S6*A*, *B*). Within the CD4+ population, we found a reduced percentage of immune-suppressive CD4+ regulatory cells (as defined by FoxP3 and CD25 marker staining) in the tumors isolated from αPD-L1/paclitaxel-treated group. CD4+FoxP3+T were dramatically affected by αPD-L1 alone as previously published (53)(*SI Appendix* Fig. S6*C*). While paclitaxel alone did not affect CD8+ population, these cells were moderately reduced in tumors from αPD-L1/paclitaxel cohort (*SI Appendix* Fig. S6*D*). To better characterize the phenotype of CD8+T cells, we stained them for CD44/CD62L markers. αPD-L1/paclitaxel-treated tumors contained a higher percentage of CD8 effector (CD_{eff}) cells than all other tumors (Fig. 5*B*,*C* and *SI Appendix* Fig. S6*E*). In the same tumors, CD8+T cells presented the highest expression of interferon-gamma (IFN-γ), granzyme-B (GrnzB), PD-1 and CD107a and, confirming their activation and cytotoxic activity in the TME (Fig. 5*D-G* and *SI Appendix* Fig.S6*F-I*).

DISCUSSION

The recent success of PD-1/PD-L1 blockade has renewed interest in immunotherapies, and in combining them with chemotherapy to achieve additive or synergistic clinical activity. Clinicians are currently exploring these combinatorial strategies for the treatment of TNBC, a very aggressive form of BC with poor prognosis. In TNBC, the expression of PD-L1 is almost undetectable in ductal carcinoma in situ (DCIS) tumor epithelial cells but increases to a higher extent in invasive ductal carcinoma (IDC) with the amplification of the CD274 locus encoding PD-L1 in about 30% of the cases(53). This important finding suggests that in TNBC, TME immune-suppressive functions progressively change during tumor evolution. Together with anthracyclines, taxanes (including paclitaxel) are currently used as first-line therapy with variable success and frequent cases of relapse(1). The expression of PD-L1 in tumor and tumor-infiltrating cells in TNBC patients suggest that PD-L1 blockade may be a useful strategy to potentiate the anti-tumor effects of taxanes. Indeed, several clinical trials are currently exploring the combination of taxanes with PD-L1 inhibitors in TNBC(52). Very

recently, the primary results of one of these trails, IMpassion130, a phase III trial of an anti-PD-L1 or anti-PD-1 antibody, have been reported in patients with metastatic TNBC(54). Although the study has not reached statistical significance yet, numerical increases in median overall survival were clearly observed in both the randomized population and in the subgroup where PD-L1 expression was assessed in tumor-infiltrating cells(54). One of the most important findings of this work is that PD-L1 expression levels in the tumor-infiltrating cells should be taken in consideration to guide treatment strategies in TNBC. Our data reporting the regulation of PD-L1 expression by paclitaxel in macrophages and TAM align with this result. Although PD-L1 expression has been generally considered to be induced at the transcriptional level after exposure to IFN-γ released by T effector cells(55), novel ways of transcriptional regulation of PD-L1 are emerging in both immune and tumor cells(19, 46). Here we have shown that in macrophages, PD-L1 levels respond to intracellular redox imbalances caused by both metabolic alterations such as deprivation of antioxidants and chemotherapy such as taxane. Overall, these data suggest a scenario where any intracellular or extracellular stresses affecting TME redox status can influence the communication between tumor cells and the surrounding immune system. In these settings, TAM responds to chemotherapy-induced ROS by upregulating PD-L1, releasing VEGF-A to promote angiogenesis and suppressing T cell mediated anti-tumor response. This suggests that administration of immunotherapy could potentiate paclitaxel efficacy by interfering with the immunosuppressive abilities of macrophages established by paclitaxel itself. Indeed, combinatorial αPD-L1 and paclitaxel therapy promotes the anti-tumoral properties of TME by significantly increasing the percentage of tumor-infiltrating effector and cytotoxic $CD8_+$T cells. Given the broad expression of PD-L1 in the TME, PD-L1 blockade may affect a wide range of cells, including tumor cells, T and B cells, natural killer, dendritic dells and macrophages(56). However, in our *in* vivo tumor model, ROS specifically increase PD-L1 in the macrophage compartment. Remarkably, it has been reported that TAM interfere with the cytotoxic activity of paclitaxel and TAM depletion potentiates the anti-tumor effect of the paclitaxel(57-59). In conclusion, our work has revealed a unique scenario that further supports the combination of PD-L1 blockade with taxane for the treatment of TNBC patients.

REFERENCES

1. Senkus E*, et al.* (2015) Primary breast cancer: ESMO Clinical Practice Guidelines for diagnosis, treatment and follow-up. *Ann Oncol* 26 Suppl 5:v8-30.

2. Liedtke C*, et al.* (2008) Response to neoadjuvant therapy and long-term survival in patients with triple-negative breast cancer. *J Clin Oncol* 26(8):1275-1281.
3. Teschendorff AE, Miremadi A, Pinder SE, Ellis IO, & Caldas C (2007) An immune response gene expression module identifies a good prognosis subtype in estrogen receptor negative breast cancer. *Genome Biol* 8(8):R157.
4. Savas P*, et al.* (2016) Clinical relevance of host immunity in breast cancer: from TILs to the clinic. *Nat Rev Clin Oncol* 13(4):228-241.
5. Banerji S*, et al.* (2012) Sequence analysis of mutations and translocations across breast cancer subtypes. *Nature* 486(7403):405-409.
6. Emens LA & Middleton G (2015) The interplay of immunotherapy and chemotherapy: harnessing potential synergies. *Cancer Immunol Res* 3(5):436-443.
7. Solinas C*, et al.* (2017) Targeting immune checkpoints in breast cancer: an update of early results. *ESMO Open* 2(5):e000255.
8. Smyth MJ, Ngiow SF, Ribas A, & Teng MW (2016) Combination cancer immunotherapies tailored to the tumour microenvironment. *Nat Rev Clin Oncol* 13(3):143-158.
9. Teng MW, Ngiow SF, Ribas A, & Smyth MJ (2015) Classifying Cancers Based on T-cell Infiltration and PD-L1. *Cancer Res* 75(11):2139-2145.
10. Kowanetz M*, et al.* (2018) Differential regulation of PD-L1 expression by immune and tumor cells in NSCLC and the response to treatment with atezolizumab (anti-PD-L1). *Proc Natl Acad Sci U S A* 115(43):E10119-E10126.
11. Conklin KA (2004) Chemotherapy-associated oxidative stress: impact on chemotherapeutic effectiveness. *Integr Cancer Ther* 3(4):294-300.
12. Jezierska-Drutel A, Rosenzweig SA, & Neumann CA (2013) Role of oxidative stress and the microenvironment in breast cancer development and progression. *Adv Cancer Res* 119:107-125.
13. Cassetta L & Kitamura T (2018) Targeting Tumor-Associated Macrophages as a Potential Strategy to Enhance the Response to Immune Checkpoint Inhibitors. *Front Cell Dev Biol* 6:38.
14. Carron EC*, et al.* (2017) Macrophages promote the progression of premalignant mammary lesions to invasive cancer. *Oncotarget* 8(31):50731-50746.
15. Hartley G, Regan D, Guth A, & Dow S (2017) Regulation of PD-L1 expression on murine tumor-associated monocytes and macrophages by locally produced TNF-alpha. *Cancer Immunol Immunother* 66(4):523-535.
16. Griffith OW & Meister A (1979) Glutathione: interorgan translocation, turnover, and metabolism. *Proc Natl Acad Sci U S A* 76(11):5606-5610.
17. Murray PJ (2017) Macrophage Polarization. *Annu Rev Physiol* 79:541-566.
18. Mantovani A*, et al.* (2004) The chemokine system in diverse forms of macrophage activation and polarization. *Trends Immunol* 25(12):677-686.
19. Prima V, Kaliberova LN, Kaliberov S, Curiel DT, & Kusmartsev S (2017) COX2/mPGES1/PGE2 pathway regulates PD-L1 expression in tumor-associated macrophages and myeloid-derived suppressor cells. *Proc Natl Acad Sci U S A* 114(5):1117-1122.
20. Ruffell B*, et al.* (2014) Macrophage IL-10 blocks CD8+ T cell-dependent responses to chemotherapy by suppressing IL-12 expression in intratumoral dendritic cells. *Cancer Cell* 26(5):623-637.
21. Makita N, Hizukuri Y, Yamashiro K, Murakawa M, & Hayashi Y (2015) IL-10 enhances the phenotype of M2 macrophages induced by IL-4 and confers the ability to increase eosinophil migration. *Int Immunol* 27(3):131-141.
22. Aras S & Zaidi MR (2017) TAMeless traitors: macrophages in cancer progression and metastasis. *Br J Cancer* 117(11):1583-1591.

23. Wang N*, et al.* (2018) CXCL1 derived from tumor-associated macrophages promotes breast cancer metastasis via activating NF-kappaB/SOX4 signaling. *Cell Death Dis* 9(9):880.
24. Holen I*, et al.* (2016) IL-1 drives breast cancer growth and bone metastasis in vivo. *Oncotarget* 7(46):75571-75584.
25. Spiegel A*, et al.* (2016) Neutrophils Suppress Intraluminal NK Cell-Mediated Tumor Cell Clearance and Enhance Extravasation of Disseminated Carcinoma Cells. *Cancer Discov* 6(6):630-649.
26. Tatano Y, Shimizu T, & Tomioka H (2014) Unique macrophages different from M1/M2 macrophages inhibit T cell mitogenesis while upregulating Th17 polarization. *Sci Rep* 4:4146.
27. Elgueta R*, et al.* (2009) Molecular mechanism and function of CD40/CD40L engagement in the immune system. *Immunol Rev* 229(1):152-172.
28. Grohmann U*, et al.* (2001) Positive regulatory role of IL-12 in macrophages and modulation by IFN-gamma. *J Immunol* 167(1):221-227.
29. Ma X*, et al.* (2015) Regulation of IL-10 and IL-12 production and function in macrophages and dendritic cells. *F1000Res* 4.
30. Noy R & Pollard JW (2014) Tumor-associated macrophages: from mechanisms to therapy. *Immunity* 41(1):49-61.
31. Rogakou EP, Pilch DR, Orr AH, Ivanova VS, & Bonner WM (1998) DNA double-stranded breaks induce histone H2AX phosphorylation on serine 139. *J Biol Chem* 273(10):5858-5868.
32. Brown SB & Savill J (1999) Phagocytosis triggers macrophage release of Fas ligand and induces apoptosis of bystander leukocytes. *J Immunol* 162(1):480-485.
33. Tardaguila M*, et al.* (2013) CX3CL1 promotes breast cancer via transactivation of the EGF pathway. *Cancer Res* 73(14):4461-4473.
34. Morgan MJ & Liu ZG (2011) Crosstalk of reactive oxygen species and NF-kappaB signaling. *Cell Res* 21(1):103-115.
35. Natoli G & Chiocca S (2008) Nuclear ubiquitin ligases, NF-kappaB degradation, and the control of inflammation. *Sci Signal* 1(1):pe1.
36. Kishore N*, et al.* (2003) A selective IKK-2 inhibitor blocks NF-kappa B-dependent gene expression in interleukin-1 beta-stimulated synovial fibroblasts. *J Biol Chem* 278(35):32861-32871.
37. Bristow CL*, et al.* (2008) NF-kappaB signaling, elastase localization, and phagocytosis differ in HIV-1 permissive and nonpermissive U937 clones. *J Immunol* 180(1):492-499.
38. Vogel CF*, et al.* (2014) Cross-talk between aryl hydrocarbon receptor and the inflammatory response: a role for nuclear factor-kappaB. *J Biol Chem* 289(3):1866-1875.
39. Goode G, Pratap S, & Eltom SE (2014) Depletion of the aryl hydrocarbon receptor in MDA-MB-231 human breast cancer cells altered the expression of genes in key regulatory pathways of cancer. *PLoS One* 9(6):e100103.
40. Terashima J, Tachikawa C, Kudo K, Habano W, & Ozawa S (2013) An aryl hydrocarbon receptor induces VEGF expression through ATF4 under glucose deprivation in HepG2. *BMC Mol Biol* 14:27.
41. Cheng CS*, et al.* (2011) The specificity of innate immune responses is enforced by repression of interferon response elements by NF-kappaB p50. *Sci Signal* 4(161):ra11.
42. Ghisletti S*, et al.* (2010) Identification and characterization of enhancers controlling the inflammatory gene expression program in macrophages. *Immunity* 32(3):317-328.

43. Becht E*, et al.* (2016) Estimating the population abundance of tissue-infiltrating immune and stromal cell populations using gene expression. *Genome Biol* 17(1):218.
44. Gorrini C*, et al.* (2014) Estrogen controls the survival of BRCA1-deficient cells via a PI3K-NRF2-regulated pathway. *Proc Natl Acad Sci U S A* 111(12):4472-4477.
45. Rom-Jurek EM*, et al.* (2018) Regulation of Programmed Death Ligand 1 (PD-L1) Expression in Breast Cancer Cell Lines In Vitro and in Immunodeficient and Humanized Tumor Mice. *Int J Mol Sci* 19(2).
46. Samanta D*, et al.* (2018) Chemotherapy induces enrichment of CD47(+)/CD73(+)/PDL1(+) immune evasive triple-negative breast cancer cells. *Proc Natl Acad Sci U S A* 115(6):E1239-E1248.
47. Peng J*, et al.* (2015) Chemotherapy Induces Programmed Cell Death-Ligand 1 Overexpression via the Nuclear Factor-kappaB to Foster an Immunosuppressive Tumor Microenvironment in Ovarian Cancer. *Cancer Res* 75(23):5034-5045.
48. Chung W*, et al.* (2017) Single-cell RNA-seq enables comprehensive tumour and immune cell profiling in primary breast cancer. *Nat Commun* 8:15081.
49. Azizi E*, et al.* (2018) Single-Cell Map of Diverse Immune Phenotypes in the Breast Tumor Microenvironment. *Cell* 174(5):1293-1308 e1236.
50. Chuang YY*, et al.* (2002) Gene expression after treatment with hydrogen peroxide, menadione, or t-butyl hydroperoxide in breast cancer cells. *Cancer Res* 62(21):6246-6254.
51. Kwa MJ & Adams S (2018) Checkpoint inhibitors in triple-negative breast cancer (TNBC): Where to go from here. *Cancer* 124(10):2086-2103.
52. Soliman HH (2017) nab-Paclitaxel as a potential partner with checkpoint inhibitors in solid tumors. *Onco Targets Ther* 10:101-112.
53. Gil Del Alcazar CR*, et al.* (2017) Immune Escape in Breast Cancer During In Situ to Invasive Carcinoma Transition. *Cancer Discov* 7(10):1098-1115.
54. Schmid P*, et al.* (2018) Atezolizumab and Nab-Paclitaxel in Advanced Triple-Negative Breast Cancer. *N Engl J Med*.
55. Yamazaki T*, et al.* (2002) Expression of programmed death 1 ligands by murine T cells and APC. *J Immunol* 169(10):5538-5545.
56. Gibbons Johnson RM & Dong H (2017) Functional Expression of Programmed Death-Ligand 1 (B7-H1) by Immune Cells and Tumor Cells. *Front Immunol* 8:961.
57. Olson OC, Kim H, Quail DF, Foley EA, & Joyce JA (2017) Tumor-Associated Macrophages Suppress the Cytotoxic Activity of Antimitotic Agents. *Cell Rep* 19(1):101-113.
58. DeNardo DG*, et al.* (2009) CD4(+) T cells regulate pulmonary metastasis of mammary carcinomas by enhancing protumor properties of macrophages. *Cancer Cell* 16(2):91-102.
59. DeNardo DG*, et al.* (2011) Leukocyte complexity predicts breast cancer survival and functionally regulates response to chemotherapy. *Cancer Discov* 1(1):54-67.
60. Barish GD*, et al.* (2010) Bcl-6 and NF-kappaB cistromes mediate opposing regulation of the innate immune response. *Genes Dev* 24(24):2760-2765.
61. Alexandrov LB, Nik-Zainal S, Wedge DC, Campbell PJ, & Stratton MR (2013) Deciphering signatures of mutational processes operative in human cancer. *Cell Rep* 3(1):246-259.
62. Barbie DA*, et al.* (2009) Systematic RNA interference reveals that oncogenic KRAS-driven cancers require TBK1. *Nature* 462(7269):108-112.

Materials and Methods

Mice

K14cre BRCA1$^{f/f}$ p53$^{f/f}$ (KBP) mice were provided by Dr. J. Jonkers (NKI, Amsterdam, The Netherlands) and were on the FVB background. KBP tumor cells were obtained and used for *in vivo* transplantation studies as previously described(44). For KBP transplantation studies, FVB recipient female mice were 8-10 week old and were purchased from The Jackson Laboratory. Mice were maintained and handled according to protocols approved by the Animal Care and Use Committee of the University Health Network (UHN; Toronto, Canada).

Preparation of murine bone marrow-derived macrophages (BMDM)

Whole bone marrow was harvested from 10-12 weeks old female mice by flushing Hanks' Balanced Salt Solution (HBSS) through femurs and tibias using a 27-gauge needle (BD Biosciences). Following red blood cell lysis, cells were cultured in 10% RPMI in 10cm plates overnight. Non-adherent cells were collected and seeded in petri dishes in medium containing 20 ng/ml mouse macrophage colony-stimulating factor (M-CSF; PeproTech). After 3 days of culture, cell media was replenished with media containing 20ng/ml M-CSF. Macrophages were harvested on day 4 and used for all the *in vitro* assays described in the manuscript. Polarization toward alternative-activated macrophages was obtained by culturing BMDM with medium containing 20 ng/ml IL-4 (PeproTech) and 20 ng/ml M-CSF (PeproTech) for 24 h. For co-culture experiments, BMDM ($1x10^6$) were seeded in triplicate in 6-well plates and incubated with or without KBP cells ($2.5x10^5$ cells/well). Cells were harvested 24h later using enzyme-free cell dissociation medium (Millipore) and sorted on an Astrios FACS Instrument (Beckman Coulter).

Preparation of human macrophages

To generate human macrophages, CD14-positive monocytes were isolated from PBMCs from healthy donors (obtained from the Princess Margaret Cancer Center blood donor center) using human CD14 microbeads (Miltenyi Biotech). Monocytes were cultured in DMEM plus 10 % FBS (Gibco), and 100 U/ml penicillin and streptomycin in the presence of recombinant human M-CSF (PeproTech) at 50ng/ml. After 5-7 days, the differentiated macrophages were characterized by flow cytometry and used in all the reported experiments.

KBP mammary tumor induction and treatment

KBP cells ($3x10^5$) were transplanted into #4 mammary gland fat pads of syngeneic female FVB recipient mice (10 weeks old). Diameters of developing tumors were measured in duplicate using digital calipers starting on day 14 post-transplantation. Tumor volume (mm^3) was calculated as ½(width^2 * height). Tumor diameters were measured, and volumes

calculated as above three times per week. For experiments with Paclitaxel, anti-PD-L1 antibody (10F.9G2; BioXCell) or Isotype Control (LTF-2; BioXCell) antibodies, KBP transplanted female mice were monitored until tumors reached a volume of 70mm^3 and randomized. Mice were injected intravenously with Paclitaxel (20mg/kg, Medkoo) or vehicle (saline) once a week. When needed, the same mice were administrated with mouse anti-PD-L1 antibody (200μg/mouse) or its isotype control (200μg/mouse) twice a week intraperitoneally. Paclitaxel was purchased in a powder form and dissolved in a solution of ethanol/cremophor EL/1X PBS (1:1:18). Both anti-PD-L1 and isotype antibodies were diluted in appropriate dilution buffers that were provided by the manufacturer.

Mouse mammary tumor dissociation

Tumors were resected from #4 mammary fat pads of transplanted mice, cut into 2-3mm^2 pieces, and placed into a C-tube (Miltenyi Biotech) containing 5 ml Iscove's Modified Dulbecco's Medium (IMDM) supplemented with 10% FBS, 2 mM L-glutamine, 100 U/ml penicillin, 100 μg/ml streptomycin, 0.05 mM β-mercaptoethanol, 0.26 U/ml Liberase TM (Sigma), and 20 U/ml DNase I (Sigma). Tumors were mechanically processed using a gentleMACS Octo Dissociator with Heaters (Miltenyi Biotech). Processed samples were filtered once through a 100 μm cell strainer (Falcon), and the corresponding C-tubes were rinsed with 5 ml cold IMDM and passed through the same strainer. Cells were filtered once using a 70 μm strainer (Falcon), followed by a 40 μm strainer (Falcon). Filtered samples were collected in 15 ml Falcon tubes and centrifuged at 1250 RPM for 8 min at 4°C. Pellets were incubated with red blood cell lysis buffer for 7 min at room temperature (RT), and then centrifuged at 1250 RPM for 8 min at 4°C before resuspension in 1X PBS-/- containing 1% bovine serum albumin (BSA) plus 2 mM ethylenediaminetetraacetic acid (EDTA). Cell suspensions were subjected to fluorescence-activated cell sorting (FACS)/flow cytometry as described below.

Flow cytometry

For mouse tumor-associated macrophages and BMDM, cell surface marker staining for flow cytometry analysis was performed using the following antibodies (Abs), all from BioLegend unless indicated: anti-CD49f (AF488 GoH3; 1/200), anti-CD45.1 (AF700 A20; 1/400), anti-CD11b (Pacific Blue M1/70; 1/400), anti-F4/80-PE (BM8; 1/400), anti-F4/80-PerCP-Cy5.5 (BM8; 1/200), anti-MHC II (I_A/I_E)-PE (M5/114.15.2; 1/1600; Thermo Fisher Scientific), anti-CD206-AF647 (C068C2; 1/400), anti-PD-L1-Pe-Cy7 (10F.9G2; 1/400), anti-CD3-AF488 (145-2C11; 1/250), anti-CD8-APC-Cy7 (53-6.7; 1/200), anti-CD4-PerCP-Cy5.5 (RM4-5; 1/800), anti-CD25-PE (PC61; 1/200), anti-IFNγ-APC (XMG1.2; 1/200), anti-Granzyme B-PE

(GB11; 1/200), anti-TNFα-PE-Cy7 (MP6-XT22; 1/800), anti-CD107a-BV421 (1D4B; 1/800), anti-CD62L-PE-Cy7 (MEL-14; 1/800; Thermo Fisher Scientific), anti-CD44-APC (IM7; 1/800) and anti-PD1-PE (RMP1-30; 1/200; Thermo Fisher Scientific).

For IFN-γ and GranzimeB staining, cells were stimulated with phorbol myristate acetate (PMA) (20 ng/ml, Sigma) and ionomycin (1 ug/m, Sigma) in presence of the intracellular protein transport inhibitor Brefeldin A (eBioscience). Cells were harvested 5h later and stained for surface markers as following. Cells were washed twice with 1X PBS-/-, fixed and permeabilized on ice for 30min with Intracellular Permeabilization kit (Thermo Fisher Scientific). After washing with the permeabilization buffer, cells were stained for IFN-γ and GranzimeB on ice for 30min.

Mouse macrophages were identified as $CD49f^{lo/-}CD45^{+}CD11b^{+}F4/80^{hi}$ and mouse T cells as $CD49f^{lo/-}CD45^{+}CD3^{+}$. Mouse macrophages were treated with Mouse BD Fc Block™ (anti-CD16/CD32 2.4G2; eBioscience) at 1/100 dilution for at least 10 min prior staining with appropriate Abs. For human macrophages, cell surface marker staining was performed with PDL1 BV421 (29E.2A3; 1/400) and CD11b BV510 (ICRF44; 1/400), both from BioLegend.

Human macrophages were treated with 1X PBS-/- containing 5% BSA and 2 mM EDTA for 30 min on ice prior staining with Abs. For both mouse and human macrophages, Abs were prepared at the indicated dilutions in 1X PBS-/- containing 1% BSA and 2 mM EDTA for 30 min on ice. Dead cells were excluded by adding 5 µl of 7-AAD (BioLegend) during the last 10 min of staining with the Abs. Cells were then washed twice and further analyzed.

To quantify intracellular cytokine production, mouse mammary tumor cells suspensions were treated with phorbol myristate acetate (PMA) (5 ng/ml, Sigma) and ionomycin (500 ng/m, Sigma) in presence of the intracellular protein transport inhibitor Brefeldin A (eBioscience) and Monensin (eBioscience), for 4 hours prior to staining. The cells were fixed and permeabilized prior to immunostaining for IL-12 PE (C15.6; 1/400; BD), IL-17 (TC11-18H10.1; 1/400; BioLegend) and IL-10 (JES5-16E3; 1:400; BioLegend). Positivity were assessed among live $CD45^{+}CD11b^{+}F4/80^{+}$ cells. All samples were analyzed at Fortessa Instrument (BD Biosciences) and data were processed with FlowJo (Tree Star, Inc.) and GraphPad software.

Analysis of peripheral blood monocytes

Peripheral blood (15µl) was first collected from mouse tail vein into heparinized capillary tubes, and then transferred into a 5 ml polystyrene tube containing 100 µl 1X PBS-/- plus 20 mM EDTA. After blocking with anti-CD16/CD32 abs (1:100) for 10 min, samples were stained with anti-CD11b-Pacific Blue and anti-PD-L1-PE-Cy7 as described above. Samples

were washed twice 1X PBS-/- containing 1% BSA and 2 mM EDTA. Red blood cells were lysed at room temperature for 10 min with 1ml of Fix/Lyse solution (ThermoFisher). Cells were washed twice with 1X PBS-/- and analyzed at Fortessa Instrument (BD Biosciences). Data were processed with FlowJo (Tree Star, Inc.) and GraphPad software.

Phospho-P65 staining by flow cytometry

Tumors were dissociated according to mouse mammary tumor dissociation method. 10_6cells were suspended in 0.5 ml of 1X PBS and immediately fixed with 0.5 ml of 4% formaldehyde (final concentration 2%) at 37°C for 10 min. Cells were washed by centrifugation with 1X PBS-/- containing 1% BSA and 2 mM EDTA prior staining with anti-CD45.1 (AF700 A20; 1/400), anti-CD11b (Pacific Blue M1/70; 1/400), anti-F4/80 (PE BM8; 1/400), anti-CD206 (Fitc C068C2; 1/400) and anti-PD-L1 (Pe-Cy7 10F.9G2, 1/400) (see flow cytometry method for additional details). Cells were washed twice with 1X PBS-/- containing 1% BSA and 2 mM EDTA and permeabilized by slowly adding ice-cold Perm Buffer II (eBioscience) with gentle vortexing. Cells were incubated on ice for 30 min and washed twice. Cells were then suspended in 100ul of primary phospho-p65 (Ser536) antibody (93H1, 1/1600, Cell signaling) or isotope control (rabbit IgG, 1/1600, Thermo Fisher Scientific) and incubated on ice for 1h. After two washes, cells were resuspended in 100ul of secondary antibody (goat anti-rabbit APC coniugated, Thermo Fishes Scientific) diluted 1/500 and incubated on ice for 1h. Cells were then washed twice and analyzed at Fortessa Instrument (BD Bioscience) and data were processed with FlowJo software (Tree Star, Inc.).

Phospho-P65 staining by immunofluorescence

For analysis of p65 S536 phosphorylation, $2x10_5$ BMDM were seeded in a 12 well plate containing glass coverslips. The day after, cells were treated with BSO (200μM) and Paclitaxel (100nM) in the presence or absence of SC514 (50μM) for 3h. Cell treatment with Lipopolysaccharide (LPS) at 1mg/ml for 30min was included as positive control of p65 S536 phosphorylation. After treatments, cells were fixed with 4% PFA for 15 min at 37°C. Cells were then stained overnight at 4°C with primary antibody (93H1, 1:1600, Cell Signaling). The following day, cells were washed three times and subjected to FITC-conjugated secondary antibody (A-11008, Thermo Fisher Scientific) at 1:1000 for 2hr RT. Nuclei were counterstained with DAPI (P36962, Thermo Fisher Scientific). To quantify phospho-p65 nuclear fluorescence intensity, we randomly selected 100 nuclei for each sample and analyzed them with ImageJ software as following. First, we applied an otsu threshold to the DAPI channel to generate a mask marking the nuclear area. Then, with the tracing tool, we

transpose each mask to the FITC-positive channel to calculate the Mean Intensity in the nuclear region.

Cell lines and treatments

Mouse KBP cells were cultured in DMEM/F12 medium containing 10% FBS (Thermo Fisher Scientific), L-glutamine, 1 µg/ml hydrocortisone (Sigma), 5 µg/ml insulin (Sigma), 5 ng/ml epidermal growth factor (EGF, Sigma) and penicillin-streptomycin (Pen-Strep, ThermoFisher Scientific). Human macrophages were cultured in DMEM medium supplemented with 10% FBS (Thermo Fisher Scientific), L-glutamine and penicillin-streptomycin (Pen-Strep, Thermo Fisher Scientific). The glutathione synthesis inhibitor, buthionine sulfoximine (BSO, Sigma) was used at 200 µM (BMDM) or 1mM (human macrophages) for specific period of times as indicated in the main manuscript. Chemotherapeutic drugs were administered *in vitro* at the following concentrations: 100nM (Paclitaxel, Medkoo), 0.5µM (Olaparib, Medkoo) and 2µM (Cisplatin, Medkoo). Anti-PD-L1 mouse or Isotype control antibodies were both used at 10µg/ml (BioXCell). For ROS scavenging, BSO or paclitaxel-exposed cells were co-treated with 1mM NAC (SIGMA). The NF-kB antagonist SC514 (Sigma) was applied to cell cultures at 50µM**.** The AhR inhibitor, CH-223191 (MedKoo) was used at 10µM for 24h.

Sulforhodamine B (SRB) colorimetric assay

BMDM were seeded at 8000cells/well in triplicate. The day after, cells were treated with Paclitaxel at 100nM or DMSO for 24h. The following day, anti-PD-L1 or isotype control antibodies were added to the cells at 10µg/ml. Cells were stained with Sulforhodamine B every 24h and processed accordingly to the manufacturer's recommendations. Cell density was calculated using the SoftMax Pro software (Molecular Devices).

Mouse Cytokine array

Mouse Cytokine Antibody Array kit (Abcam) was performed to measure chemokines, cytokines and growth factors in the culture media of BMDM and according to manufacturer's instructions. Membranes were developed for chemiluminescent detection and images were acquired with GelCapture Software using MicroChemi 2.0/4.2 (FroggaBio).

RT-PCR

RNA was isolated using the Nucleospin RNA Plus kit (Macherey-Nagel) and reverse-transcribed using the iScript cDNA synthesis kit (Bio-Rad) according to manufacturers' instructions. Quantitative RT-PCR was performed using SYBR Green primers (Applied Biosystems). Mouse and human ribosomal proteins S9 (rps9) were used as housekeeping

genes to calculated relative mRNA expression. All mouse and human primer sequences are described in *SI Appendix* Table 1.

Chromatin Immunoprecipitation

Chromatin immunoprecipitation (ChIP) assay was performed using SimpleChip® Plus Enzymatic Chromatin IP Kit (#9003, Cell Signaling Technology). $8 \times 10_6$ BMDM were left untreated or treated with 100nM paclitaxel with or without 1mM NAC for 1 h. Chromatin was prepared by enzymatic shearing according to the manufacturer's instructions. Immunoprecipitation was performed at 4°C overnight with 0.75µg NF-κB p65 Ab (L8F6, Cell Signaling) and 1µg mouse IgG as negative control. Following immunoprecipitation, samples were incubated with Chip-Grade protein G Magnetic Beads from Kit at 4°C for 2 h. The cross-linking was reversed by adding 5 M NaCl and proteinase K at 65°C for 2 h. Real-time PCR was performed on DNA isolated from each ChIP reactions (n=3) using Power SYBR Green PCR master mix. Primers are indicated in *SI Appendix* Table 1.

ROS measurement

To measure intracellular ROS, $2x10_5$ BMDM were incubated with 300 nM CM-H_2DCFDA (DCF-DA, C6827, Invitrogen) for 10 min at 37°C. DCF-DA fluorescence was analyzed by flow cytometry using a FACS Fortessa (BD Biosciences) and data were processed with FlowJo software.

DNA damage measurement

To measure intracellular DNA damage, $2x10_5$ BMDM were fixed and permeabilized with BD Cytofix/Cytoperm (BD Biosciences). Then, cells were stained with FITC-conjugated γ-H2AX (1/400; Millipore) for 1h, washed twice and analyzed by flow cytometry using a FACS Fortessa (BD Biosciences). Data were processed with FlowJo software.

Immunohistochemistry

Tissue sections were cut from frozen tissue specimens in OCT 8-10um thick. Slides were dried overnight and immunohistochemistry performed the next day. Slides were briefly washed in PBS followed by 15min in 0.3% hydrogen peroxide-PBS to quench endogenous peroxidases. Slides were then washed in PBS before applying a histoblock solution (HB: BSA, MgCl2, 0.2% Tween20) for 30min. Slides were drained and anti-p65 antibody (93H1, 1:100, Cell Signaling) was applied and incubated overnight at 4C. The following day, slides were washed and secondary Ab applied for 30min (goat anti-rabbit secondary, BA-1000, VectorLabs). ABC reagent (PK-6100, VectorLabs) was applied for 25min following development with DAB (SK-4100, VectorLabs). Specimens were viewed with a brightfield

microscope (Leica DM2500 equipped with Micropublisher 3.3-QI imaging camera) using Q-Capture Pro Software and processed with Adobe Photoshop CS5.

Cleaved caspase 3 staining

Tissue specimens from treated mouse cohorts were processed for cleaved caspase 3 immunohistochemical staining as following. Antigen retrieval was perfomed with microwave heating in 10mM Na citrate (pH 6.0) treatment for 25 min. The primary Ab was prepared in histoblock solution (3% BSA, 20mM $MgCl_2$,0.3% Tween 20 in 1X PBS with 5% goat serum with 0.2% Triton X-100 at a dilution of 1:1000 overnight at 4^{o}C. Secondary Ab (goat anti-rabbit, Vector labs BA-4001) was incubated for 1h min at a dilution of 1:400. Signal was visualized with DAB Peroxidase reagent (Vector labs kit SK-4100). Slides were digitized using a Nanozoomer2.0 HT-Hamamatsu (Olympus). An image analysis protocol (APP) was developed using Visiopharm software (Visiopharm, Denmark) to identify the cells that were positive for cleaved caspase 3. A ratio of positive cells to total cell number was then calculated for each slide.

Analysis of mouse BMDM databases

Unsupervised clustering of *Pdl1*, *Nfkb1/p65*, and *Rela/p50* gene expression profiles in mouse BMDM exposed to LPS (data from GEO reference GSE27112) (41). The Spearman's correlation coefficients (SCCs) of *Cd274* and the two other genes are shown. Mouse genomic region including the *Pdl1* gene and depicting the Nfkb1/p65 chromatin immunoprecipitation results in BMDM untreated or exposed to LPS (two assays indicated in yellow and green; GEO reference GSE16723)(60). The positions of the Nfkb1/p65 enhancer described in Ghisletti et al. 2010 and validated by ChIP-qPCR is also indicated in blue(42).

Analysis of human breast cancer datasets

In TCGA database, Pam50 calls annotated in clinical data were used to identify primary breast tumors of the basal subtype. HR-deficient BC cohort was defined by using TCGA breast cancer RNAseq data and somatic mutations after being obtained following approval by the Data Access Committee (project #11689). The results published here are partly based upon data generated by TCGA managed by the National Cancer Institute and the National Human Genome Research Institute. Information about TCGA can be found at http://cancergenome.nih.gov. Mutational signatures were defined using the R mut Signatures package(61). The expression signature scores were computed using the ssGSEA algorithm with standard parameters and using all genes included in each set(62).

The PCC and p-values were computed in R, and immune cell types were inferred using the Microenvironment Cell Populations-counter (MCP-counter) method(43). The "Chuang_oxidative_stress_response" gene set (ROS up-regulated genes only) was chosen because it includes a highly comprehensive gene expression signature derived from the cellular response to three different oxidants, including hydrogen peroxide, menadione, and t-butyl hydroperoxide(50).

Statistical analyses

Data were reported in bar graphs as the mean or median ± standard error of the mean (SEM), with p-values calculated using Student's t-test (*≤0.05, **≤0.01, ***≤0.001). The mean was calculated based on a minimum of n=3 replicates in each experiment, and each experiment was performed at least 3 times. Data were analyzed either by Microsoft Excel or GraphPad Prism 7.

AUTHOR CONTRIBUTIONS

C.R. designed and performed experiments, analyzed data and co-wrote the paper; S.J. performed experiments and analyzed data; R.S. performed experiments with human macrophages and provided technical assistance in the analysis of immune system; D.W.C, J.S., M.F., K.H., G.D. and A.W. provided technical support and supervised *in vivo* mouse studies; L.P., M.G. and M.A.P. performed bioinformatic analysis; T.B. analyzed immunohistochemical specimens; T.W.M. gave conceptual advice; T.L.M. gave conceptual advice and contributed to the design of immune system analysis; P.C. gave conceptual advice, contributed to the design of the experiments and wrote the paper; C.G. conceived the project, designed experiments and wrote the paper.

ACKNOWLEDGEMENTS

This study was supported by Susan G. Komen Career Catalyst Research Grant 410005437 (C.G.); Foundation CIHR grant Funding Reference Number 143268 (T.W.M.); Carlos III Institute of Health grants PI15/00854 and PI18/01029, co-funded with European Union ERDF funds (FEDER) (M.A.P.); Generalitat de Catalunya grant 2017-449 (M.A.P.); CERCA program (M.A.P.); Italian Ministry of University and Research (Miur) (P.C.); University of Turin-Progetti Ricerca Locale (P.C.) and National Cancer Institute/National Institute of Health Grant CA190449 (T.L.M). We thank Andrew Elia for assistance in

immunohistochemical staining, Kelsie Thu, Christian Bassi and Shawn P. Kubli for helpful discussions and technical advice.

FIGURE LEGENDS

Figure 1: ROS regulate PD-L1 expression and secretion of immunosuppressive cytokines in BMDM. (*A*) *Pdl1* mRNA levels in BMDM obtained from FVB mice (n=4/group). Cells were left untreated (Ctrl) or treated for 24h with BSO (200μM)±NAC (1mM). (*B*) *Gclc* and *Gclm* mRNA levels in BMDM treated as in (*A*). n=4/group. (*C, D*) Percentage of PD-L1 positive BMDM gated on live $CD45_+$ $CD11b_+$ $F4/80_+$ within $CD206_+$MHC-II_- (*C*) or $CD206_-$MHC-II_+ (*D*) populations. Cells were isolated from n=3 FVB mice and analyzed after being treated as in (*A*). (*E)* Levels of indicated chemokines in the supernatant of BMDM, as determined by cytokine antibody array after treatment with BSO (200μM)±NAC (1mM) for 24h. Values are the mean of biological duplicates and are represented as ratio to untreated control. (*F*) *Pdl1* mRNA levels in BMDM that were exposed to DMSO (Ctrl) or paclitaxel (100nM)±NAC (1mM) for 24h. n=4/group. *G*) *Gclc* and *Gclm* mRNA levels in BMDM treated as in (*F*). (*H, I*) Percentage of PD-L1 positive BMDM gated on live $CD45_+$ $CD11b_+$ $F4/80_+$ within $CD206_+$MHC-II_- (*H*) or $CD206_-$MHC-II_+ (*I*) populations. Cells were isolated from n=3 mice treated as in (*F*). (*J*) Levels of indicated chemokines in the supernatant of BMDM as determined by cytokine antibody array and treated as in (*F*). Values are the mean of biological duplicates and are represented as ratio to DMSO-treated control cells. Data in A-D and F-I are presented as mean ± S.E.M of biological replicates. $^*P \leq 0.05$, $^{**}P \leq 0.01$,$^{***}P \leq 0.001$.

Figure 2: ROS-induced PD-L1 expression is mediated by the transcription factor NF-kB. (*A*) Relative number of cells containing p65 S536 phosphorylation (P-p65) as assessed by immunofluorescence staining of BMDM that were treated with DMSO (Ctrl) and BSO (200μM) or paclitaxel (100nM) ± SC514 (50μM) or NAC (1mM). Cells stimulated with LPS for 30min were used as positive control. n=4 slides/group. A total number of 100 cells were counted in each slide. The bar graph represents the mean of all values ± S.E.M. (*B*) Nuclear signal intensity of P-p65 in cells treated and presented as in (*A*). See Material & Methods for additional details. (C) *IkBa* mRNA levels in BMDM treated as in (*A*). (*D*) *Pdl1* mRNA levels in BMDM left untreated or treated with DMSO (Ctrl) and BSO (200μM) or paclitaxel (100nM) ± SC514 (50μM). (*E*)

Percentage of PD-L1 positive BMDM gated on live $CD45_+$ $CD11b_+$ $F4/80_+$ within $CD206_+$MHC-II_- cells after being treated as in (*D*). (*F*) Scheme showing NF-kB1/p65 binding sites on mouse *Pdl1* promoter region as found through bioinformatic analysis of GSE16723 and Ghisletti et al. 2010 datasets. Yellow and green indicates two biological replicates of LPS-treated BMDM. The location of NF-kB1/p65 binding enhancer from Ghisletti et al. 2010 is indicated in blu. (*G*) ChIP-qPCR showing a peak of enrichment of p65 at I1551 enhancer in *Pdl1* promoter region in BMDM treated with BSO for 1h. NAC reverted the BSO-mediated effect. n=3. Data in C-E and G are presented as mean ± S.E.M of biological replicates. *P≤0.05, **P≤0.01,***P≤0.001.

Figure 3: Paclitaxel promotes PD-L1 expression in tumor-associated macrophages *in vivo*. (*A*) Percentage of PD-L1 positive cells gated on live $CD49f_-$ $CD45_+$ $CD11b_+$ $F4/80_+$ $CD206_+$ cells isolated from KBP tumors (n=5/group) after 24h and 5 days of treatment with paclitaxel (20mg/kg) or vehicle (saline). (*B*) Percentage of PD-L1 positive cells gated on live $CD49f_-$ $CD45_+$ $CD11b_+$ $F4/80_-$ cells from peripheral blood of KBP-bearing mice treated as in (*A*). n=5/group. (*C*) ROS intracellular measurement by DCF-DA staining of live $CD45_+$ $CD11b_+$ $F4/80_+$ cells, gated accordingly to PD-L1 negative ($PD\text{-}L1_-$) or positive surface expression ($PD\text{-}L1_+$). Cells were isolated from KBP tumors after 5 days of treatment with paclitaxel (20mg/kg). n=6/group. (*D*) Percentage of PD-L1 positive cells ($PD\text{-}L1_+$) gated on live $CD49f_+$ $CD45_-$ cells isolated from KBP tumors (n=5/group) after 24h and 5 days of treatment with paclitaxel or its vehicle. (*E-G*) Analysis of intracellular production of IL-10 (*E*), IL-17 (*F*) and IL-12 (*G*) in CD11b+F4/80+ isolated from vehicle- and paclitaxel-treated tumors at 5 day post-treatment. n=5. (*H*) Flow cytometric analysis of S536 phosphorylation in p65 in TAM isolated from tumor-bearing mice ($CD49f_{low/-}CD45_+$ $CD11b_+$ $F4/80_+$ $CD206_+$ $PD\text{-}L1_+$) at 5 days after treatment with paclitaxel or vehicle (n=6/group). Values are normalized on phospho-p65 levels in isotype control in both groups. (*I*) Positive correlation between M1 or M2 gene expression signatures (as determined by Chung et al, 2018 and Azizi et al., 2018) and the expression levels of CD274, p65/NFKB1 and the "Chuang oxidative stress response" gene signature in the TCGA human basal-like BC cohort. See Material and Methods for details. Data in A-H are presented as mean ± S.E.M of biological replicates. *P≤0.05, **P≤0.01.

Figure 4: PD-L1 blockade potentiates anti-tumor effects of paclitaxel *in vivo*. (*A*) Levels of indicated chemokines in BMDM after treatment with vehicle, paclitaxel (100nM) with αPD-L1 antibody (10μg/ml) or isotype control (10μg/ml) for 24h. Values are the mean of biological duplicates and are represented as ratio to control cells treated with DMSO and isotype. (*B*) *Vegfa* mRNA levels in BMDM treated as in (*A*). (*C*) Schematic representation of paclitaxel and αPD-L1 treatment schedule for KBP tumor-bearing mice. Control group received vehicle and isotype. (*D*) Volume measurement of mammary tumors over time in mice transplated with KBP cells and treated accordingly to the regimen described in (*C*). (*E*) Weight of tumors isolated at humane endpoint post-treatment (day 14_{th}). n=10-15/group. (*F*) Mitotic index by direct counting of mitotic cells in haematoxylin and eosin (H&E)-stained tumor sections. n=5/group. (*G*) Mean of P-p65 signal calculated as Optical Density by ImageJ assessed by immunohistochemistry of KBP tumors. n=5/group. (*H*) Quantification of cleaved caspase 3 staining performed by immunohistochemistry of KBP tumors. n=10/group. Data in B-H are presented as mean ± S.E.M of biological replicates. *P≤0.05, **P≤0.01, ***P≤0.001.

Figure 5: Paclitaxel and PD-L1 blockade combinatorial treatment promotes anti-tumor immune respose. (*A*) Percentage of $CD11b_+$ $F4/80_+$ cells gated on live $CD49f_-$ $CD45_+$ cells isolated from KBP tumors at endpoint. n=10-15/group. (*B*) Percentage of $CD8_+$ T cells gated on $CD49f_-$ $CD45_+$ $CD3_+$cells in control or treated cohorts (n=10-15/group). Cells were characterized based on the expression of CD44 and CD62L as following: naïve ($CD44_-$ $CD62L_+$), memory ($CD44_+$ $CD62L_+$) or effector ($CD44_+$ $CD62L_-$). Percentages are represented as stacked bar graphs. For the $CD8_+$ effector cells, statistical significance was determined by student t-test: vehicle+isotype versus paclitaxel+αPD-L1 (*p=0.01), vehicle+αPD-L1 versus paclitaxel+αPD-L1 (*p=0.0152), paclitaxel+isotype versus paclitaxel/αPD-L1 (**p=0.006). (*C*) Absolute numbers of $CD8_+$ effector cells in control and treated cohorts (n=10-15/group). (*D-G*) Percentage of $CD8_+$ T cells (gated on $CD49f_-$ $CD45_+$ $CD3_+$) that were positive for the expression of IFNγ, GrnzB, CD107a and PD-1 as indicated in control or treated cohorts (n=10-15/group). Data in A-G are presented as mean ± S.E.M of biological replicates. *P≤0.05, **P≤0.01, ***P≤0.001.

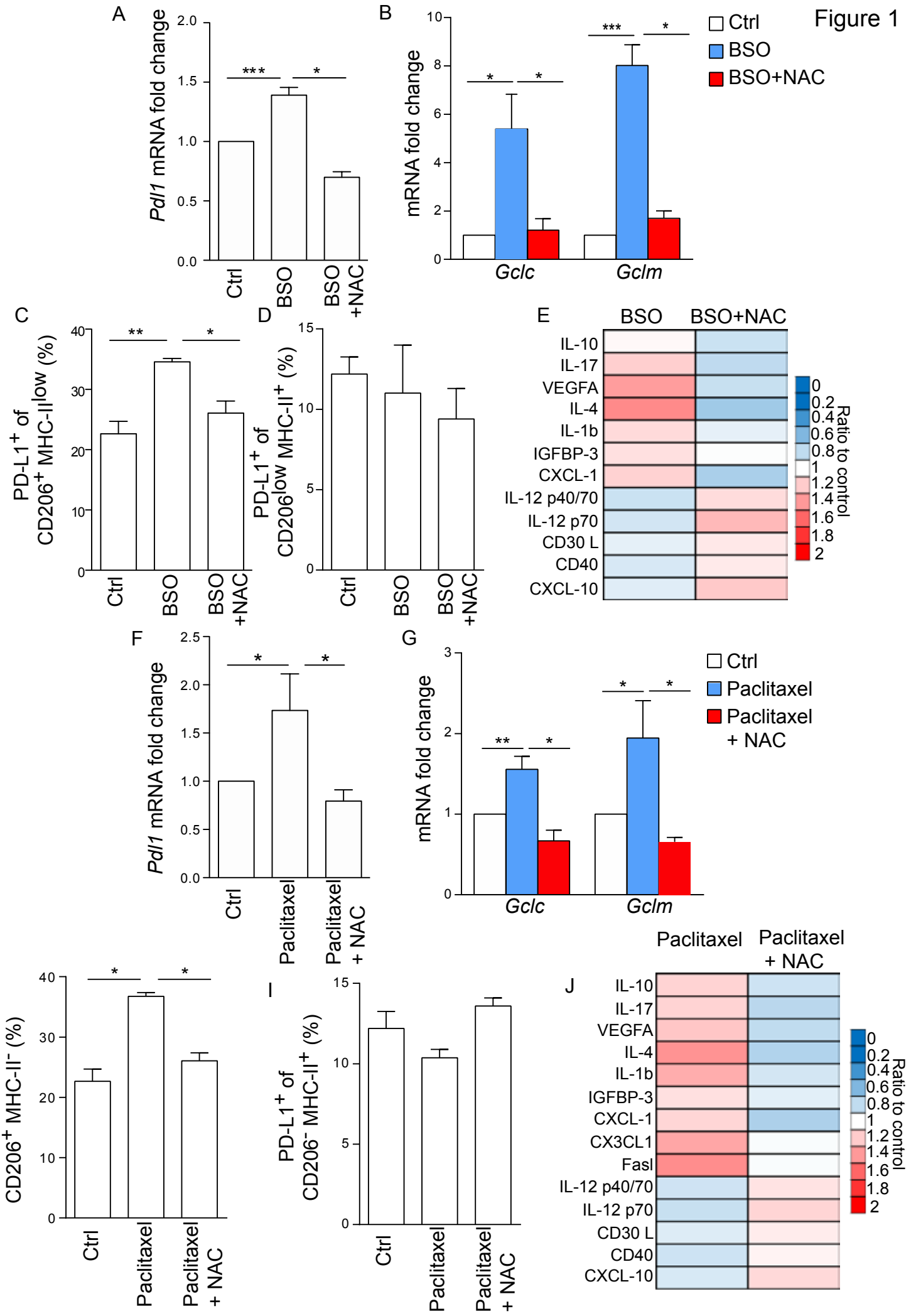
Figure 1
A
Pdl1 mRNA fold change
Ctrl
BSO
BSO +NAC
B
mRNA fold change
Ctrl
BSO
BSO+NAC
Gclc
Gclm
C
PD-L1+ of CD206+ MHC-IIlow (%)
D
PD-L1+ of CD206low MHC-II+ (%)
E
BSO
BSO+NAC
IL-10
IL-17
VEGFA
IL-4
IL-1b
IGFBP-3
CXCL-1
IL-12 p40/70
IL-12 p70
CD30 L
CD40
CXCL-10
Ratio to control
F
Pdl1 mRNA fold change
Ctrl
Paclitaxel
Paclitaxel + NAC
G
mRNA fold change
Ctrl
Paclitaxel
Paclitaxel + NAC
Gclc
Gclm
H
PD-L1+ of CD206+ MHC-II- (%)
I
PD-L1+ of CD206- MHC-II+ (%)
J
Paclitaxel
Paclitaxel + NAC
IL-10
IL-17
VEGFA
IL-4
IL-1b
IGFBP-3
CXCL-1
CX3CL1
Fasl
IL-12 p40/70
IL-12 p70
CD30 L
CD40
CXCL-10
Ratio to control

Figure 2

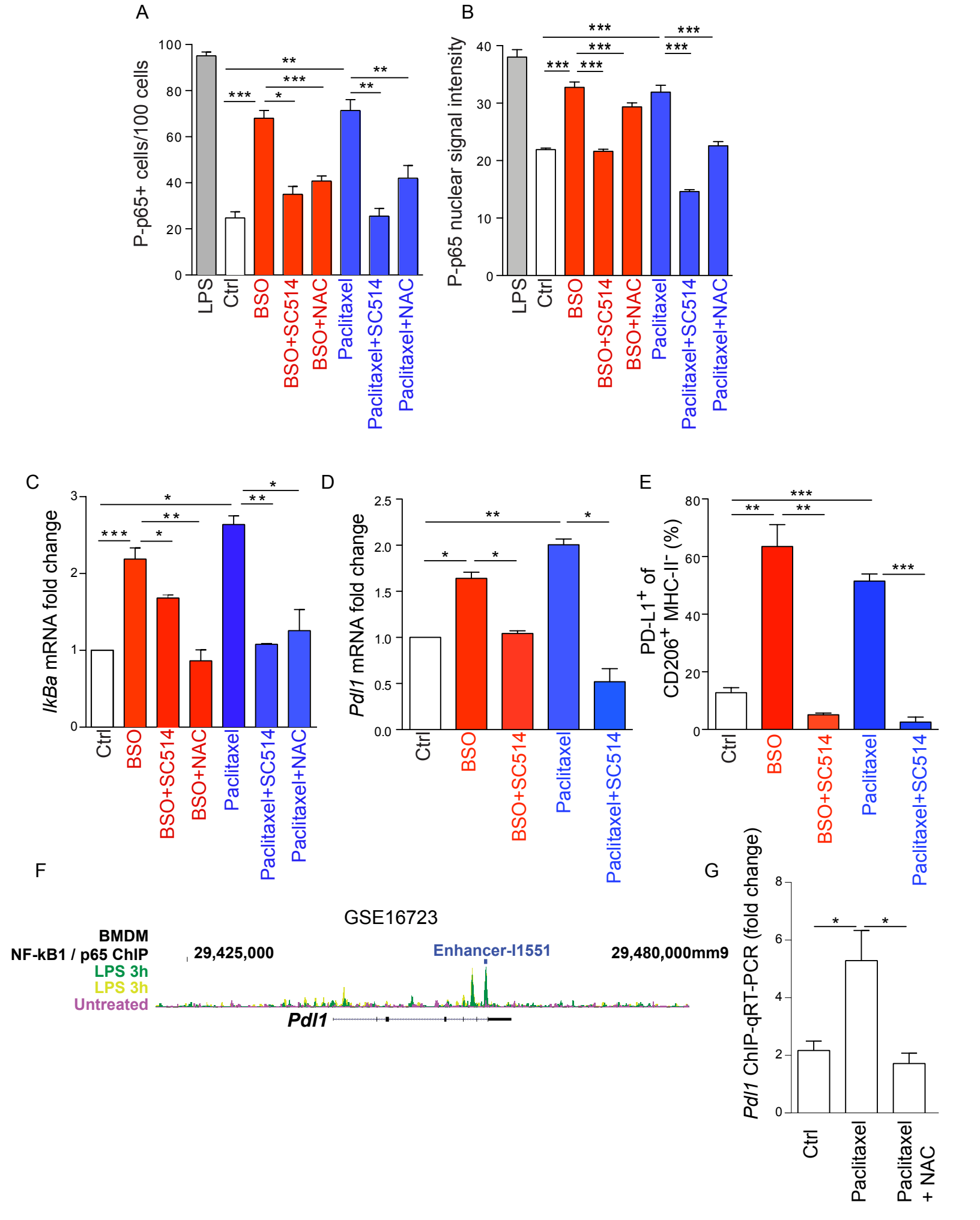
A
P-p65+ cells/100 cells
LPS
Ctrl
BSO
BSO+SC514
BSO+NAC
Paclitaxel
Paclitaxel+SC514
Paclitaxel+NAC
B
P-p65 nuclear signal intensity
C
IkBa mRNA fold change
D
Pdl1 mRNA fold change
E
PD-L1+ of CD206+ MHC-II- (%)
F
GSE16723
BMDM
NF-kB1 / p65 ChIP
LPS 3h
LPS 3h
Untreated
29,425,000
Enhancer-l1551
29,480,000mm9
Pdl1
G
Pdl1 ChIP-qRT-PCR (fold change)
Ctrl
Paclitaxel
Paclitaxel + NAC

Figure 3

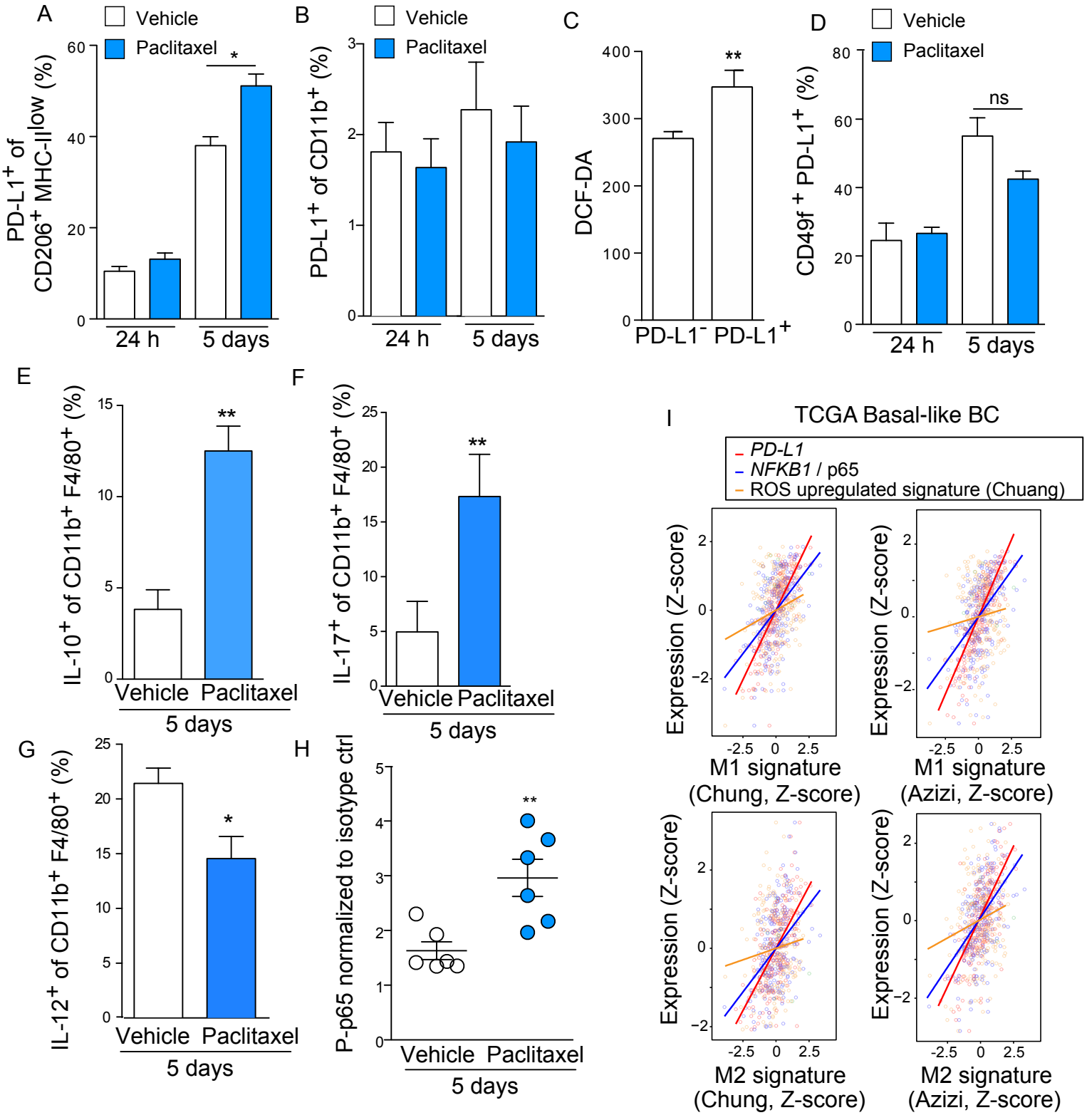
A
Vehicle
Paclitaxel
PD-L1+ of CD206+ MHC-IIlow (%)
24 h
5 days
B
PD-L1+ of CD11b+ (%)
C
DCF-DA
PD-L1- PD-L1+
D
CD49f+ PD-L1+ (%)
ns
E
IL-10+ of CD11b+ F4/80+ (%)
F
IL-17+ of CD11b+ F4/80+ (%)
G
IL-12+ of CD11b+ F4/80+ (%)
H
P-p65 normalized to isotype ctrl
I
TCGA Basal-like BC
PD-L1
NFKB1 / p65
ROS upregulated signature (Chuang)
Expression (Z-score)
M1 signature (Chung, Z-score)
M1 signature (Azizi, Z-score)
M2 signature (Chung, Z-score)
M2 signature (Azizi, Z-score)

Figure 4

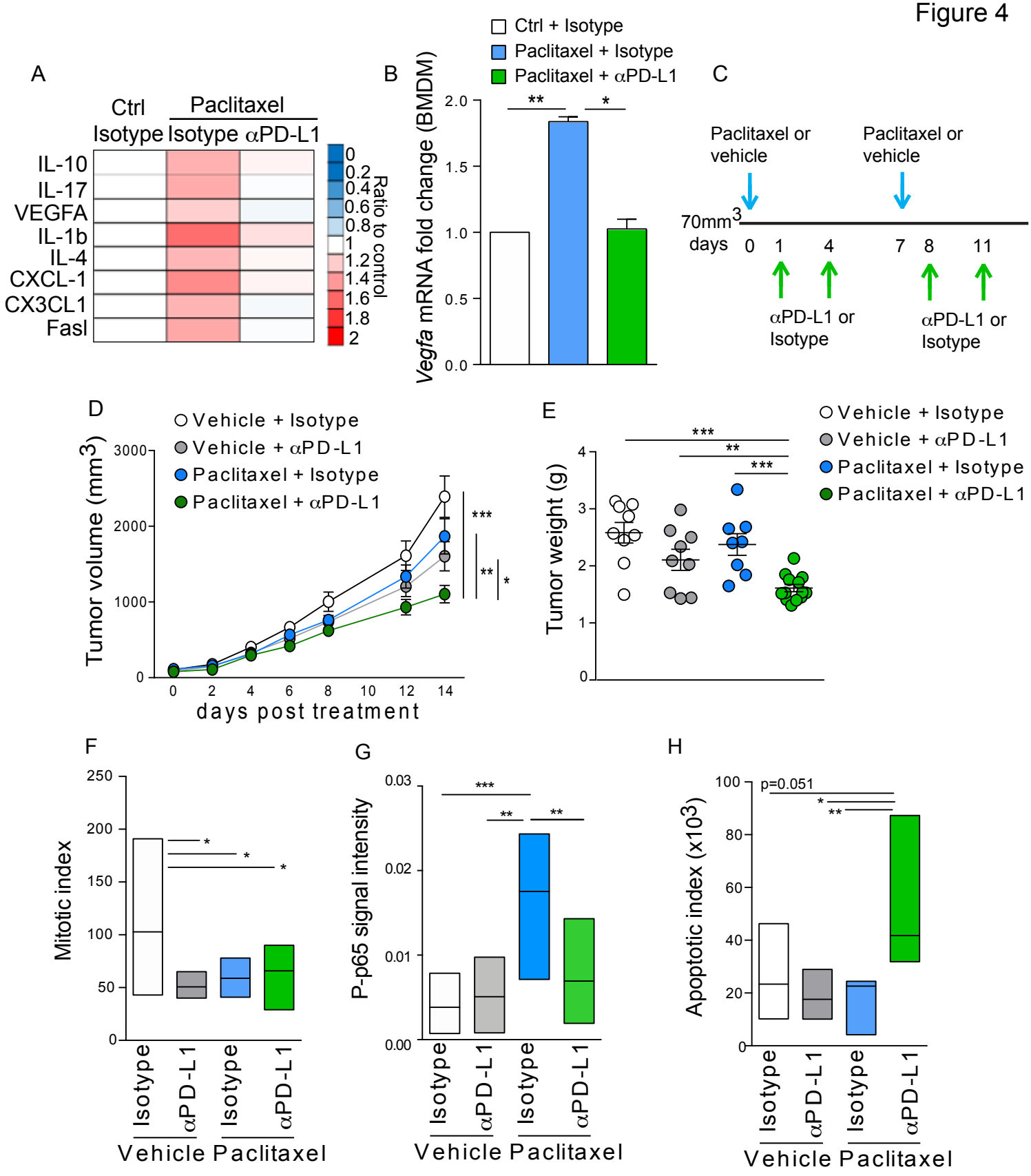
A
Ctrl
Paclitaxel
Isotype
Isotype
αPD-L1
IL-10
IL-17
VEGFA
IL-1b
IL-4
CXCL-1
CX3CL1
Fasl
Ratio to control
0
0.2
0.4
0.6
0.8
1
1.2
1.4
1.6
1.8
2
B
Ctrl + Isotype
Paclitaxel + Isotype
Paclitaxel + αPD-L1
Vegfa mRNA fold change (BMDM)
2.0
1.5
1.0
0.5
0.0
**
*
C
Paclitaxel or vehicle
Paclitaxel or vehicle
70mm3
days
0
1
4
7
8
11
αPD-L1 or Isotype
αPD-L1 or Isotype
D
Vehicle + Isotype
Vehicle + αPD-L1
Paclitaxel + Isotype
Paclitaxel + αPD-L1
Tumor volume (mm3)
3000
2000
1000
0
0
2
4
6
8
10
12
14
days post treatment
***
**
*
E
Vehicle + Isotype
Vehicle + αPD-L1
Paclitaxel + Isotype
Paclitaxel + αPD-L1
Tumor weight (g)
4
3
2
1
0
***
**
***
F
Mitotic index
250
200
150
100
50
0
*
*
*
Isotype
αPD-L1
Isotype
αPD-L1
Vehicle
Paclitaxel
G
P-p65 signal intensity
0.03
0.02
0.01
0.00
***
**
**
Isotype
αPD-L1
Isotype
αPD-L1
Vehicle
Paclitaxel
H
Apoptotic index (x103)
100
80
60
40
20
0
p=0.051
*
**
Isotype
αPD-L1
Isotype
αPD-L1
Vehicle
Paclitaxel

Figure 5

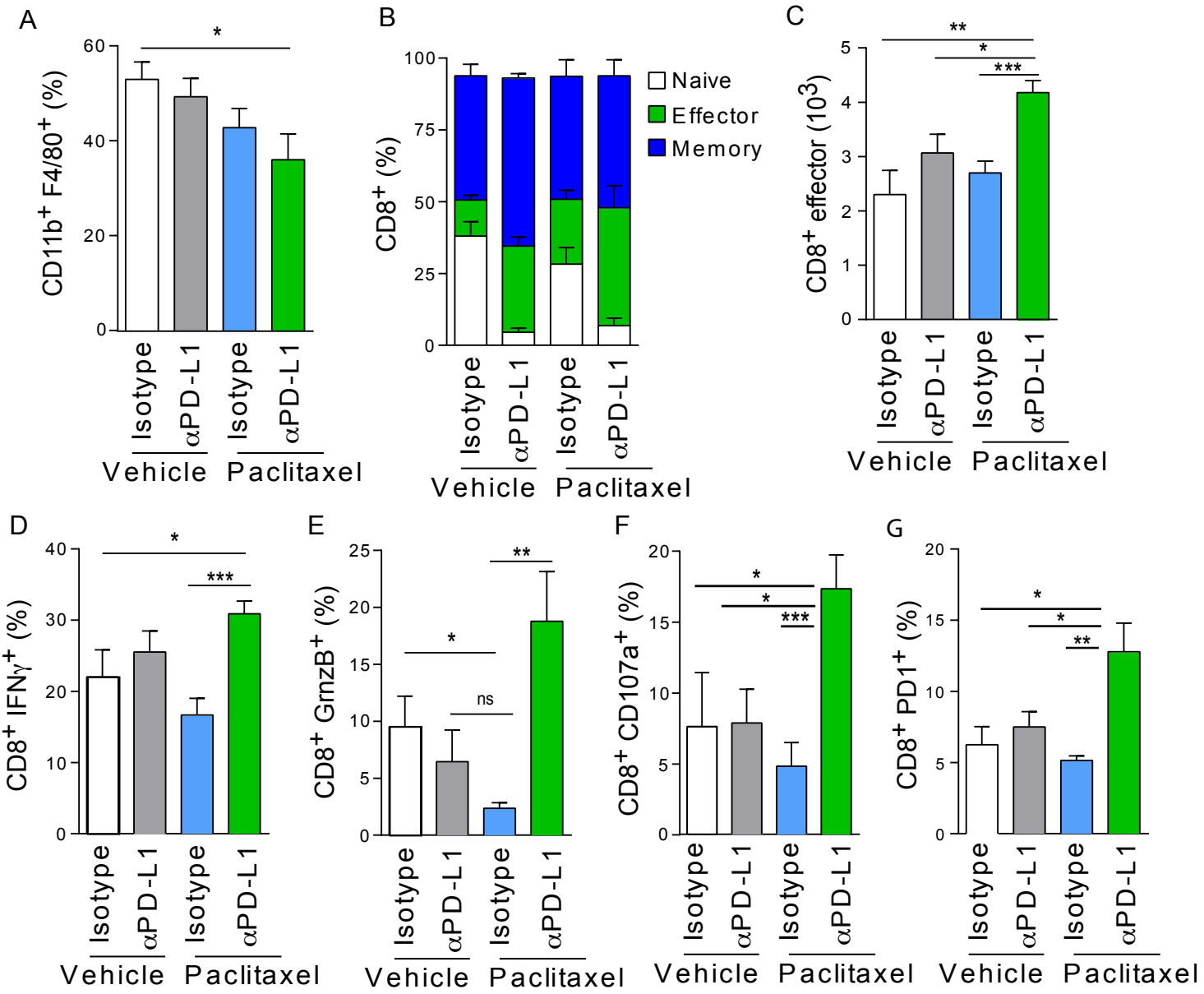
A
CD11b+ F4/80+ (%)
60
40
20
0
*
Isotype
αPD-L1
Isotype
αPD-L1
Vehicle
Paclitaxel
B
CD8+ (%)
100
75
50
25
0
Naive
Effector
Memory
Isotype
αPD-L1
Isotype
αPD-L1
Vehicle
Paclitaxel
C
CD8+ effector (10^3)
5
4
3
2
1
0
**
*
***
Isotype
αPD-L1
Isotype
αPD-L1
Vehicle
Paclitaxel
D
CD8+ IFNγ+ (%)
40
30
20
10
0
*
***
Isotype
αPD-L1
Isotype
αPD-L1
Vehicle
Paclitaxel
E
CD8+ GrnzB+ (%)
25
20
15
10
5
0
**
*
ns
Isotype
αPD-L1
Isotype
αPD-L1
Vehicle
Paclitaxel
F
CD8+ CD107a+ (%)
20
15
10
5
0
*
*
***
Isotype
αPD-L1
Isotype
αPD-L1
Vehicle
Paclitaxel
G
CD8+ PD1+ (%)
20
15
10
5
0
*
*
**
Isotype
αPD-L1
Isotype
αPD-L1
Vehicle
Paclitaxel

Figure S1

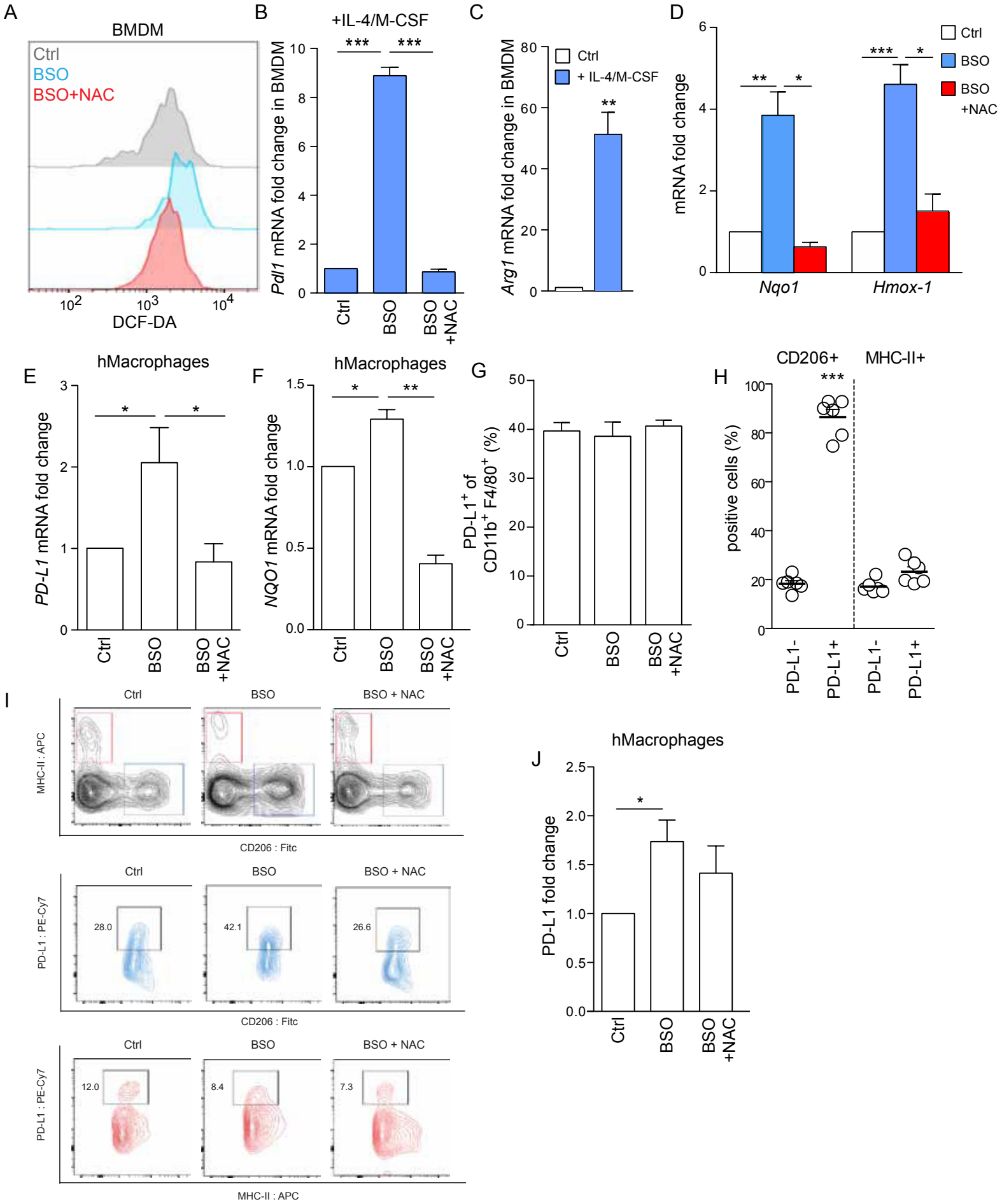
A
BMDM
Ctrl
BSO
BSO+NAC
DCF-DA
B
+IL-4/M-CSF
Pdl1 mRNA fold change in BMDM
Ctrl
BSO
BSO +NAC
C
Arg1 mRNA fold change in BMDM
Ctrl
+ IL-4/M-CSF
D
mRNA fold change
Ctrl
BSO
BSO +NAC
Nqo1
Hmox-1
E
hMacrophages
PD-L1 mRNA fold change
F
hMacrophages
NQO1 mRNA fold change
G
PD-L1+ of CD11b+ F4/80+ (%)
H
CD206+
MHC-II+
positive cells (%)
PD-L1-
PD-L1+
I
Ctrl
BSO
BSO + NAC
MHC-II : APC
CD206 : Fitc
PD-L1 : PE-Cy7
28.0
42.1
26.6
12.0
8.4
7.3
J
hMacrophages
PD-L1 fold change

Figure S2

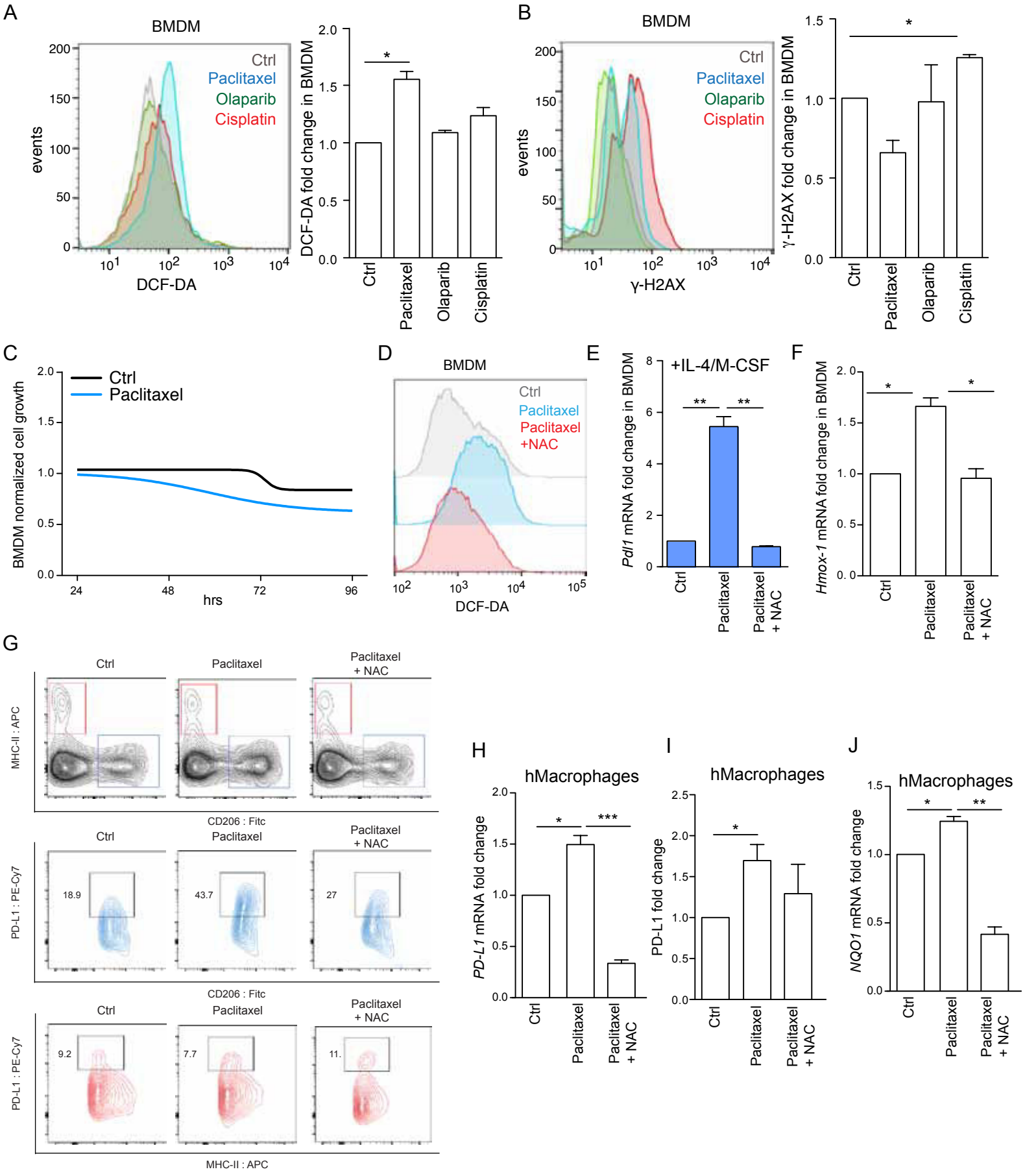
A
BMDM
Ctrl
Paclitaxel
Olaparib
Cisplatin
events
DCF-DA
DCF-DA fold change in BMDM
B
BMDM
γ-H2AX
γ-H2AX fold change in BMDM
C
Ctrl
Paclitaxel
BMDM normalized cell growth
hrs
D
BMDM
Paclitaxel +NAC
DCF-DA
E
+IL-4/M-CSF
Pdl1 mRNA fold change in BMDM
Paclitaxel + NAC
F
Hmox-1 mRNA fold change in BMDM
G
MHC-II : APC
PD-L1 : PE-Cy7
CD206 : Fitc
18.9
43.7
27
9.2
7.7
11.
H
hMacrophages
PD-L1 mRNA fold change
I
PD-L1 fold change
J
NQO1 mRNA fold change

Figure S3

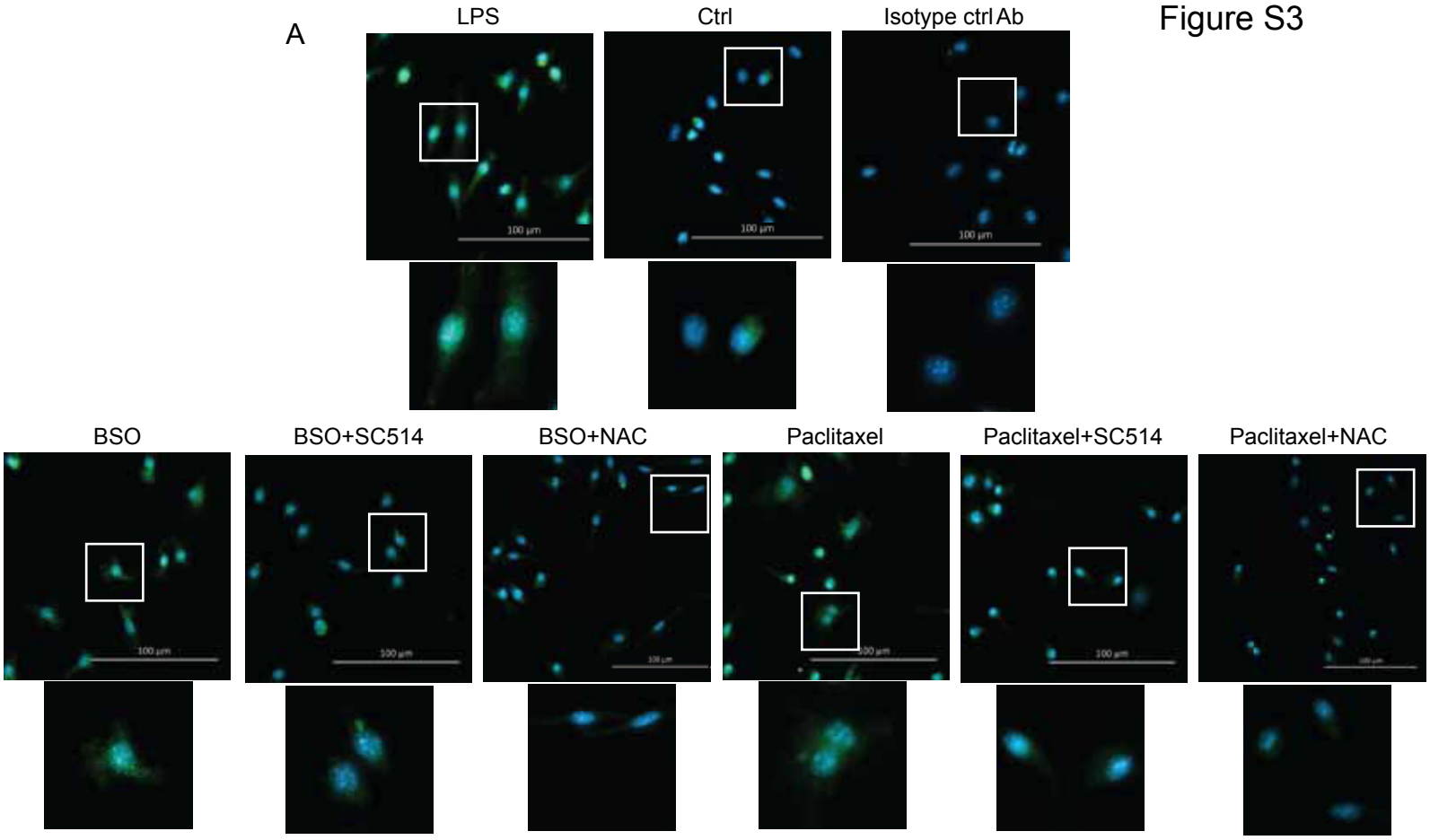
A
LPS
Ctrl
Isotype ctrl Ab
BSO
BSO+SC514
BSO+NAC
Paclitaxel
Paclitaxel+SC514
Paclitaxel+NAC

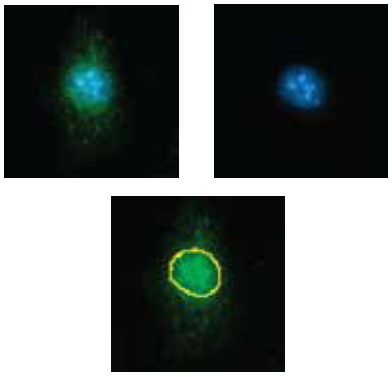
B

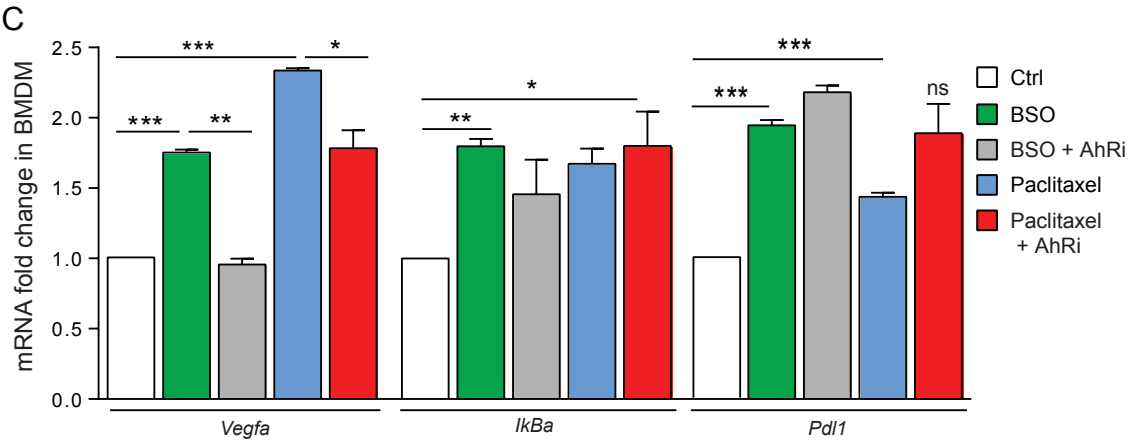
C
mRNA fold change in BMDM
2.5
2.0
1.5
1.0
0.5
0.0
***
*
**
ns
Vegfa
IkBa
Pdl1
Ctrl
BSO
BSO + AhRi
Paclitaxel
Paclitaxel + AhRi

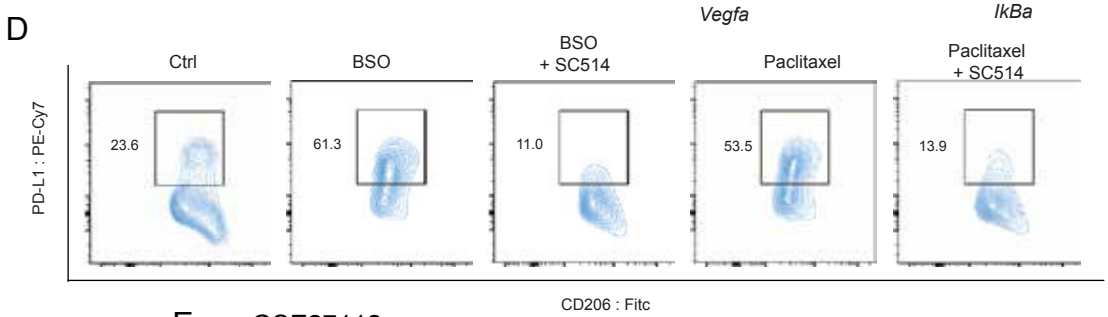
D
Ctrl
BSO
BSO + SC514
Paclitaxel
Paclitaxel + SC514
23.6
61.3
11.0
53.5
13.9
PD-L1 : PE-Cy7
CD206 : Fitc

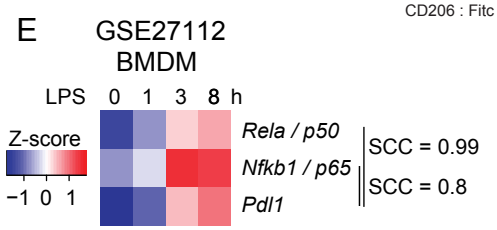
E
GSE27112
BMDM
LPS 0 1 3 8 h
Z-score
−1 0 1
Rela / p50
Nfkb1 / p65
Pdl1
SCC = 0.99
SCC = 0.8

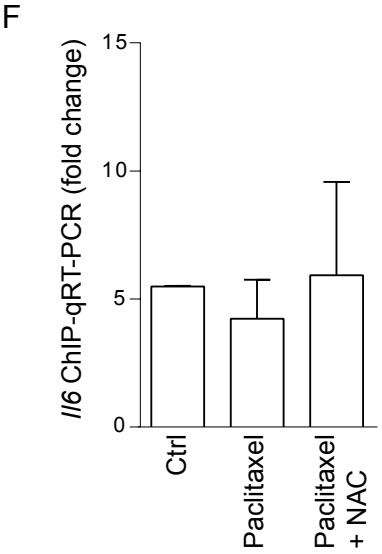
F
Il6 ChIP-qRT-PCR (fold change)
15
10
5
0
Ctrl
Paclitaxel
Paclitaxel + NAC

Figure S4

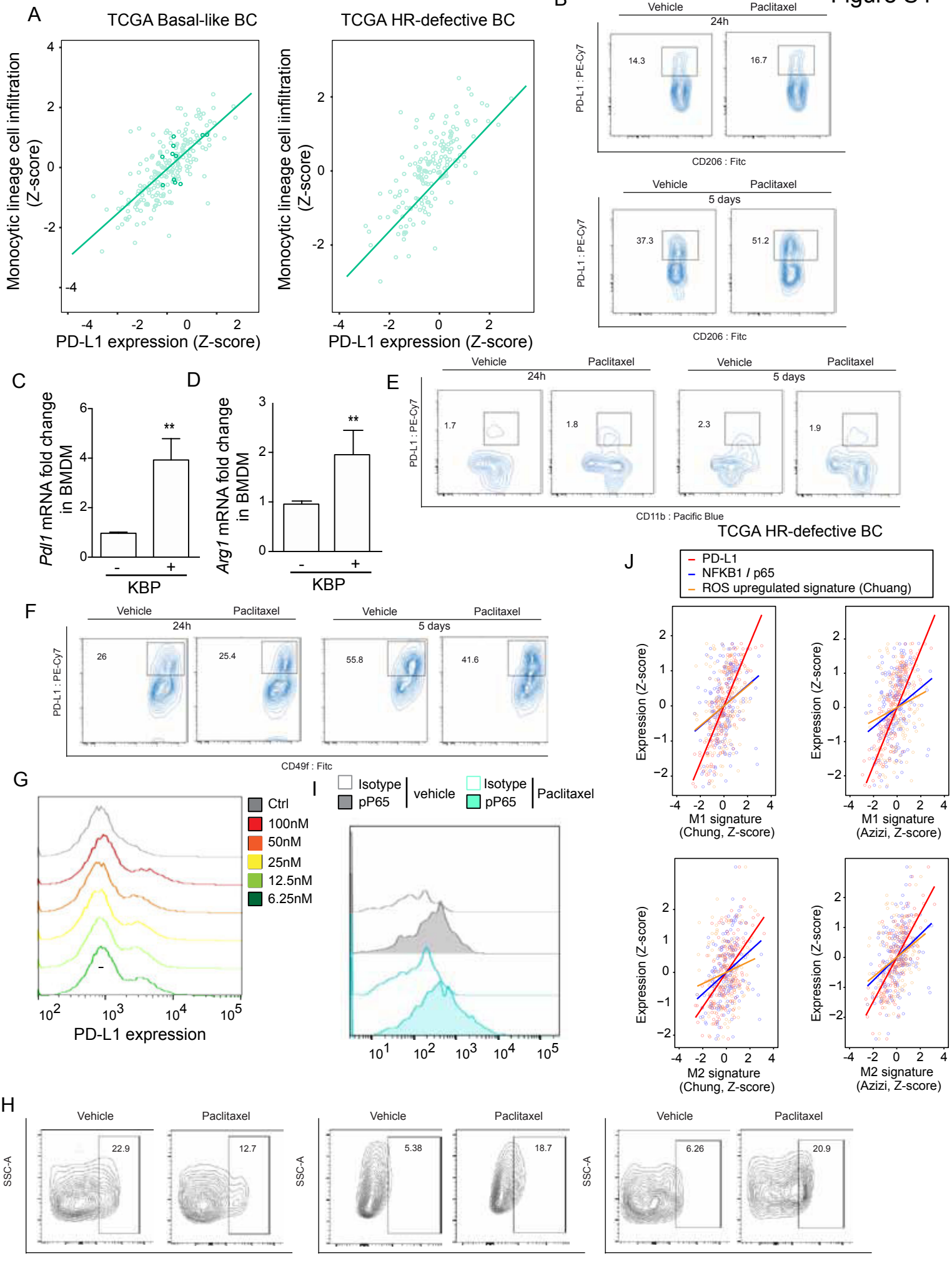
A
TCGA Basal-like BC
TCGA HR-defective BC
Monocytic lineage cell infiltration (Z-score)
PD-L1 expression (Z-score)
B
Vehicle
Paclitaxel
24h
5 days
PD-L1 : PE-Cy7
CD206 : Fitc
14.3
16.7
37.3
51.2
C
Pdl1 mRNA fold change in BMDM
KBP
D
Arg1 mRNA fold change in BMDM
E
CD11b : Pacific Blue
1.7
1.8
2.3
1.9
F
CD49f : Fitc
26
25.4
55.8
41.6
G
Ctrl
100nM
50nM
25nM
12.5nM
6.25nM
PD-L1 expression
I
Isotype
pP65
vehicle
Paclitaxel
J
TCGA HR-defective BC
PD-L1
NFKB1 / p65
ROS upregulated signature (Chuang)
M1 signature (Chung, Z-score)
M1 signature (Azizi, Z-score)
M2 signature (Chung, Z-score)
M2 signature (Azizi, Z-score)
Expression (Z-score)
H
SSC-A
IL-12 : PE
IL-17 : PE
IL-10 : APC
22.9
12.7
5.38
18.7
6.26
20.9

Figure S5

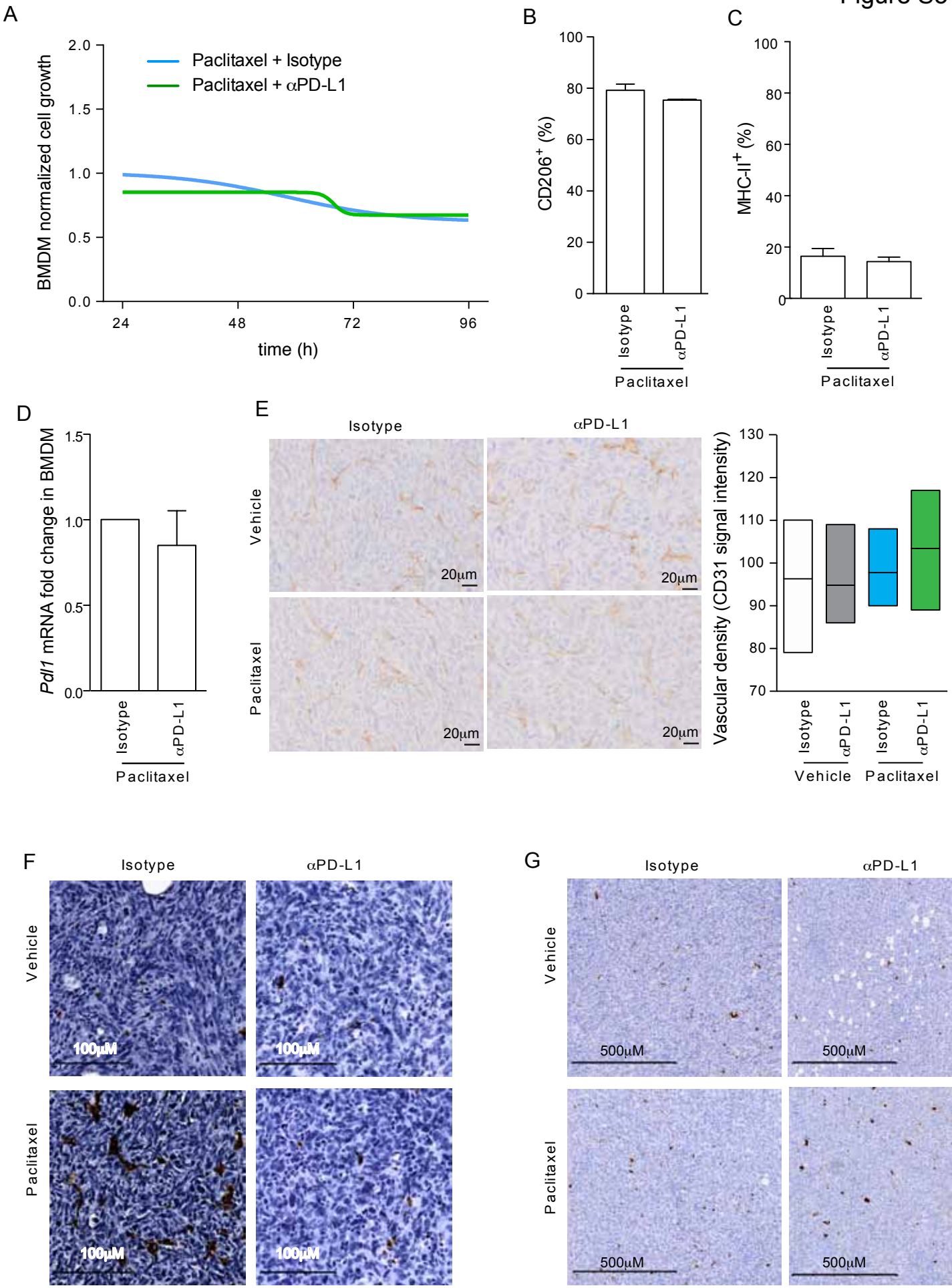
A
Paclitaxel + Isotype
Paclitaxel + αPD-L1
BMDM normalized cell growth
time (h)
B
CD206+ (%)
Isotype
αPD-L1
Paclitaxel
C
MHC-II+ (%)
Isotype
αPD-L1
Paclitaxel
D
Pdl1 mRNA fold change in BMDM
Isotype
αPD-L1
Paclitaxel
E
Isotype
αPD-L1
Vehicle
Paclitaxel
20μm
Vascular density (CD31 signal intensity)
Isotype
αPD-L1
Isotype
αPD-L1
Vehicle
Paclitaxel
F
Isotype
αPD-L1
Vehicle
Paclitaxel
100μM
G
Isotype
αPD-L1
Vehicle
Paclitaxel
500μM

Figure S6

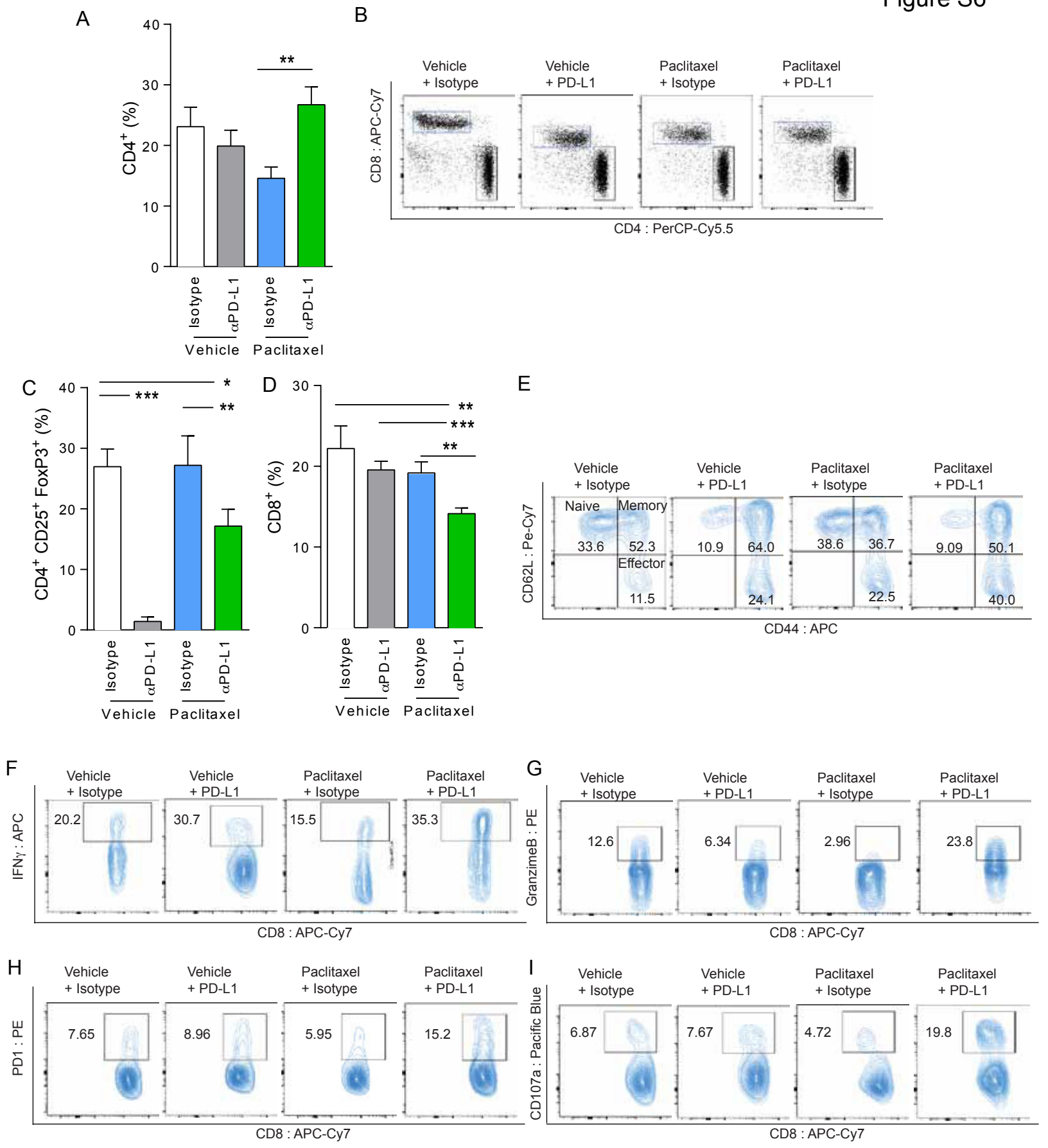
A
B
C
D
E
F
G
H
I
CD4+ (%)
Isotype
αPD-L1
Vehicle
Paclitaxel
Vehicle + Isotype
Vehicle + PD-L1
Paclitaxel + Isotype
Paclitaxel + PD-L1
CD8 : APC-Cy7
CD4 : PerCP-Cy5.5
CD4+ CD25+ FoxP3+ (%)
CD8+ (%)
CD62L : Pe-Cy7
CD44 : APC
Naive
Memory
Effector
33.6
52.3
11.5
10.9
64.0
24.1
38.6
36.7
22.5
9.09
50.1
40.0
IFNγ : APC
20.2
30.7
15.5
35.3
GranzimeB : PE
12.6
6.34
2.96
23.8
PD1 : PE
7.65
8.96
5.95
15.2
CD107a : Pacific Blue
6.87
7.67
4.72
19.8

Supplementary Table 1: Primers used for qRT-PCR and ChIP-qPCR (m=mouse) (h=human).

Gene	Primer Sequence
mRsp9 F	GCAAGATGAAGCTGGATTAC
mRps9 R	GGGATGTTCACCACCTG
mNqo1 F	AGGATGGGAGGTACTCGAATC
mNqo1 R	AGGCGTCCTTCCTTATATGCTA
mHo-1 F	AAGCCGAGAATGCTGAGTTCA
mHo-1 R	GCCGTGTAGATAATGGTACAAGGA
mGclc F	GGCTCTCTGCACC
mGclc R	GTTAGAGTACCGA
mGclm F	AAGTTAACCTGGC
mGclm R	GAGAGCAGTTCTT
mPdl1 F	CAGCAACTTCAGGGGGAGAG
mPdl1 R	TTTGCGGTATGGGGCATTGA
mIkBa F	AACCTGCAGCAGACTCCACT
mIkBa R	GACACGTGTGGCCATTGTAG
mVegfa F	CCGGGCCTCGGTT
mVegfa R	GGGACCACTTGGC
hRsp9 F	GTTTGCTTAGGCGCAGACG
hRps9 R	CCATACTCGCCGATCAGCTT
hPdl1 F	AAATGGAACCTGGCGAAAGC
hPdl1 R	GATGAGCCCCTCAGGCATTT
hNqo1 F	TCCCCCTGCAGTGGTTTGGAGT
hNqo1 R	ACTGCCTTCTTACTCCGGAAGGGT
mIL-6 F (ChIP)	CACTTCACAAGTCGGAGGCT
mIL-6 R (ChIP)	AATGAATGGACGCCCAGACT
mPdl1-I1551 F (ChIP)	GCCAGGCAGAACTAAAGTGG
mPdl1-I1551 R (ChIP)	GGTTCCTCAGGGTGACTCAG

SI APPENDIX FIGURE LEGENDS

Figure S1: ROS regulates PD-L1 mRNA and cell surface expression in BMDM. (*A*) Representative histogram profile of ROS levels in BMDM stained with DCF-DA and left untreated (Ctrl) or treated for 24h with BSO (200μM) ± NAC (1mM). n=4/group. (*B*) *Pdl1* mRNA levels in BMDM that were treated with 20ng/ml IL-4 and 20 ng/ml M-CSF (Ctr) or BSO (200μM) ± NAC (1mM). n=3/group. (*C*) *Arg1* mRNA levels in BMDM that were left untreated or treated with IL-4 and M-CSF as in (*B*). n=3/group. (*D*) *Nqo1* and *Hmox-1* mRNA levels in BMDM that were left untreated (Ctrl) or treated for 24h with BSO (200μM) ± NAC (1mM). n=4/group. (*E*) *PD-L1* mRNA levels in human macrophages that were left untreated (Ctrl) or treated for 24h with BSO (1mM) ± NAC (1mM). n=3/group. (*F*) *NQO1* mRNA levels of human macrophages treated as in (*B*). n=3/group. (*G*) Percentage of PD-L1 positive BMDM (gated on live $CD45^+$ $CD11b^+$ $F4/80^+$) that were treated as in (*E*). n=3. (*H*) Percentage of PD-L1 positive BMDM gated on live $CD45^+$ $CD11b^+$ $F4/80^+$ within $CD206^+MHC\text{-}II^-$ or $CD206^-MHC\text{-}II^+$ populations. n=3. (*I*) Representative FACS plots of PD-L1 surface staining in $CD206^+MHC\text{-}II^-$ or $CD206^-MHC\text{-}II^+$ populations treated as in (*A*). (*J*) Fold surface expression levels of PD-L1 in $CD11b^+$ human macrophages treated as in (*B*). n=3/group. Data are normalized to values from untreated cells (Ctrl). Data in B-H and J are presented as mean ± S.E.M of biological replicates. *P≤0.05, **P≤0.01, ***P≤0.001.

Figure S2: Paclitaxel-induced ROS regulates PD-L1 mRNA and cell surface expression in BMDM. (*A*) Left, representative histogram of intracellular ROS levels in BMDM as measured by DCF-DA staining. Cells were treated with DMSO (Ctrl), paclitaxel (100nM), olaparib (0.5μM) or cisplatin (2μM) for 24h. Right, quantification (n=4/group). (*B*) Left, representative histogram of DNA damage in BMDM stained for phosphorylated H2AX (γ-H2AX) and treated as in (*A*). Right, quantification (n=4/group). (*C*) SRB assay in BMDM treated for 5 days with DMSO (Ctrl) and paclitaxel (100nM). (*D*) Representative histogram profile of ROS levels in BMDM stained with DCF-DA and left untreated (Ctrl) or treated for 24h with Paclitaxel (100nM) ± NAC (1mM). n=4/group. (*E*) *Pdl1* mRNA levels in BMDM that were treated with 20ng/ml IL-4 and 20 ng/ml M-CSF (Ctr) or BSO (200μM)

± NAC (1mM). n=3/group. (*F*) *Hmox-1* mRNA levels in BMDM treated with DMSO (Ctrl) or paclitaxel (100nM) ± NAC (1mM). n=4/group. (*G*) Representative FACS plots of PD-L1 surface staining in $CD206^{+}MHC\text{-}II^{-}$ or $CD206^{-}MHC\text{-}II^{+}$ populations treated as in (*D*). (*H*) *PD-L1* mRNA levels in human macrophages that were treated for 24h with DMSO (Ctrl) or paclitaxel (100nM) ± NAC (1mM). n=3. (*I*) Surface expression levels of PD-L1 in $CD11b^{+}$ human macrophages (n=3/group). Cells were treated as in (*H*) and values normalized to control (DMSO-treated cells). (*J*) *NQO1* mRNA levels in human macrophages that were treated as in (*H*). n=3. Data in A, B, E, F and H-J are presented as mean ± S.E.M of biological replicates. *P≤0.05, **P≤0.01, ***P≤0.001.

Figure S3: ROS-regulated PD-L1 expression depends on NF-kB transcriptional activity. (*A*) Representative images of BMDM positive for S536 phosphorylated-p65 (P-p65) when treated with DMSO (Ctrl) or BSO (200mM) and paclitaxel (100nM) ± SC514 for 3h. Stimulation of BMDM with LPS for 30min was used as positive control for phosphorylated p65 (S536). The use of isotype control antibody was included as negative control. (*B*) Representative image of the analysis of P-p65 signal intensity performed by ImageJ. A mask defining the nuclear region (based on DAPI staining) was overlaid on FITC-positive image. The mean FITC signal intensity was then calculated in the defined area. (*C*) *IkBa*, *Vegfa* and *Pdl1* mRNA levels in BMDM left untreated (Ctrl) or treated with BSO (200mM) and paclitaxel (100nM)±CH-223191 (10μM) AhR inhibitor for 24h. n=3. (*D*) Representative FACS plot of PD-L1 surface expression in $CD206^{+}MHCII^{-}$ BMDM. (*E*) Spearman's correlation coefficients between mRNA expression levels of *RelA*/*p50*, *Nfkb1*/*p65* and *Pdl1* in GSE27112 dataset from BMDM that were stimulated with LPS at different time points. (*F*) ChIP-qPCR of p65 at *IL-6* promoter region in BMDM treated with BSO±NAC for 1h. n=3. Data in C and F are presented as mean ± S.E.M of biological replicates. *P≤0.05, **P≤0.01, ***P≤0.001.

Figure S4: Paclitaxel increases PD-L1 expression in tumor-associated macrophages in vivo. (*A*) Positive correlation between tumor-infiltration of monocytic lineage cells (monocyes and macrophages) and *PD-L1* expression in the TCGA human basal-like and HR-defective BC datasets. See Materials and Methods for additional

details. (*B*) Representative FACS plots of PD-L1 surface staining in TAM ($CD49f^{low/-}CD45^+$ $CD11b^+$ $F4/80^+$ $CD206^+MHC\text{-}II^{low}$) in tumors from mice treated with vehicle (saline) or paclitaxel (20mg/kg) for 24h and 5 days. (*C*,*D*) Pdl1 and Arginase1 mRNA levels in BMDM that were cultured alone or sorted after co-culture with KBP mammary tumor cells for 24h in vitro. n=3. (*E*) Representative FACS plot of PD-L1 staining in $CD11b^+$ cells from peripheral blood in tumour-bearing mice treated vehicle and paclitaxel for 24h and 5 days. (*F*) Representative FACS plot of PD-L1 staining in $CD45^-CD49f^+$ cells in tumors from mice treated vehicle and paclitaxel for 24h and 5 days. (*G*) Representative histogram of PD-L1 surface expression in KBP cells treated with the indicated doses of paclitaxel for 24h. (*H*) Representative FACS plot of IL-10, IL-17 and IL-12 in CD11b+F4/80+ cells isolated from vehicle- and paclitaxel-treated tumors at 5 days post-treatment. (*I*) Representative histogram of phospho-p65 levels in TAM ($CD49f^{low/-}CD45^+$ $CD11b^+$ $F4/80^+$ $CD206^+$ $PD\text{-}L1^+$) isolated from KBP tumors 5 days after treatment with paclitaxel or vehicle. n=6/group. (*J*) Positive correlation between M1 or M2 gene expression signatures (as determined by Chung et al, 2018 and Azizi et al., 2018) and the expression levels of *PD-L1*, *p65*/*NFKB1* and the "Chuang oxidative stress response" gene signature in the TCGA human HR-defective BC cohort. See Materials and Methods for details. Data in C and D are presented as mean ± S.E.M of biological replicates. *P≤0.05, **P≤0.01, ***P≤0.001.

Figure S5: Paclitaxel and PD-L1 blockade affects pathological features of KBP mammary tumors. (*A*) SRB cell viability assay in BMDM that were treated for 5 days with isotype control (10μg/ml) or paclitaxel (100nM)±αPD-L1 (10μg/ml). (*B, C*) Percentage of CD206 (*B*) and MHC-II (*C*) positive cells within BMDM ($CD49f^{low/-}CD45^+$ $CD11b^+$ $F4/80^+$) treated as in (*A*) for 24h. (*D*) *Pdl1* mRNA levels in BMDM treated as in (*A*). (*E*) Left, representative images of CD31-positive areas in tumors from mice treated with vehicle, isotype control, paclitaxel and αPD-L1 as indicated. Slides were counterstained with H&E. Right, quantification. n=5. (*F*) Representative images of P-p65 positive cells in tumor tissues from mice treated as in (*E*). Slides were counterstained

with H&E. (G) Representative images of cleaved caspase 3 immunostaining in tumors treated as in (*E*). Data in B-E are presented as mean ± S.E.M of biological replicates.

Figure S6: Paclitaxel and PD-L1 blockade affects the immune profile of KBP mammary tumors. (*A*) Percentage of $CD4^+$ T cells gated on live $CD49f^-$ $CD45^+$ $CD3^+$cells and isolated from KBP tumors at day 14 in mice treated with vehicle, isotype control paclitaxel and αPD-L1 as indicated. n=10-15/group. (*B*) Representative FACS plot of $CD4^+$ and $CD8^+$ population in tumors from mice treated as in (*A*). (*C*) Percentage of $FoxP3^+$ cells gated on $CD49f^-$ $CD45^+$ $CD3^+$ $CD4^+$ $CD25^+$ cells and isolated from KBP tumors at day 14 in mice treated as in (*A*). n=10-15/group. (*D*) Percentage of $CD8^+$ T cells gated on live $CD49f^-$ $CD45^+$ $CD3^+$cells isolated from KBP tumors at day 14 in mice treated as in (*A*). n=10-15/group. (*E*) Representative FACS plot of $CD8^+$ population stained for CD44 and CD62L to define naïve, memory and effector T cell subpopulations in tumors from mice treated as in (*A*). (*F-I*) Representative FACS plots showing the levels of IFN-γ, Granzyme-B, PD-1 and CD107a in $CD8^+$ population in tumors from mice treated as in (*A*). Data in A, C and D are presented as mean ± S.E.M of biological replicates. *P≤0.05, **P≤0.01, ***P≤0.001.